Genome-wide CRISPR-Cas9 screen reveals the importance of the heparan sulfate pathway and the conserved oligomeric golgi complex for synthetic dsRNA uptake and Sindbis virus infection

Olivier Petitjean[1,*], Erika Girardi[1,*], Richard Patryk Ngondo[2], Vladimir Lupashin[3], Sébastien Pfeffer[1,‡]

[1] Université de Strasbourg, Architecture et Réactivité de l'ARN, Institut de biologie moléculaire et cellulaire du CNRS, 2 allée Konrad Roentgen, 67084 Strasbourg France

[2] Université de Strasbourg, Institut de Biologie Moléculaire des Plantes du CNRS, 12 rue du Général Zimmer, 67084 Strasbourg France

[3] University of Arkansas for Medical Sciences, 4301 West Markham Street, Little Rock, Arkansas 72205, United States of America

* These authors contributed equally. Author order was determined on the basis of increasing seniority.

‡ To whom correspondence should be addressed: spfeffer@unistra.fr

Abstract

Double stranded RNA (dsRNA) is the hallmark of many viral infections. dsRNA is produced either by RNA viruses during replication or by DNA viruses upon convergent transcription. Synthetic dsRNA is also able to mimic viral-induced activation of innate immune response and cell death. In this study, we employed a genome-wide CRISPR-Cas9 loss of function screen based on cell survival in order to identify genes implicated in the host response to dsRNA. By challenging HCT116 human cells with either synthetic dsRNA or Sindbis virus (SINV), we identified the heparan sulfate (HS) pathway as a crucial factor for dsRNA entry and we validated SINV dependency on HS. Interestingly, we uncovered a novel role for COG4, a component of the Conserved Oligomeric Golgi (COG) complex, as a factor involved in cell survival to both dsRNA and SINV in human cells. We showed that COG4 knock-out led to a decrease of extracellular HS, specifically affected dsRNA transfection efficiency and reduced viral production, explaining the increased cell survival of these mutants.

Importance

When facing a viral infection, the organism has to put in place a number of defense mechanisms in order to clear the pathogen from the cell. At the early phase of this preparation for fighting against the invader, the innate immune response is triggered by the sensing of danger signals. Among those molecular cues, double-stranded (dsRNA) is a very potent inducer of different reactions at the cellular level that can ultimately lead to cell death. Using a genome-wide screening approach, we set to identify genes involved in dsRNA entry, sensing and apoptosis induction in human cells. This allowed us to determine that the heparan sulfate pathway and the Conserved Oligomeric Golgi complex are key determinants allowing entry of both dsRNA and viral nucleic acid leading to cell death.

48 **Introduction**

49 Upon infection by a virus, numerous mechanisms are put in place at the cellular level to raise
50 the alarm and get rid of, or at least limit, the invader. One of the first barrier that the virus has
51 to overcome to is to enter the cell by taking advantage of wide diversity of ubiquitous or cell-
52 specific cellular receptors. In addition to protein receptors, glycosaminoglycans present at the
53 cell surface also represent crucial factors for efficient viral attachment and entry (1).
54 Glycosaminoglycans, and more precisely heparan sulfates are ubiquitously expressed in human
55 cells. They possess a global negative charge that is able to interact electrostatically with the
56 basic residues that are exposed by viral surface glycoproteins. This allows viruses to increase
57 their concentration at cell surface and so the possibility to interact with their specific entry
58 receptor (2). For instance, alphaviruses such as Semliki Forest virus (SFV) and Sindbis virus
59 (SINV) are enveloped positive-strand RNA viruses that contain two glycoproteins at the
60 envelope, the proteins E1 and E2. E2 is involved in the interaction of the virus particle to the
61 cell surface (3, 4), while E1 serves in the fusion process (5).

62 Once inside the cell, the replication of the viral genome represents another critical step to trigger
63 the antiviral immune response. Double-stranded (ds) RNA is a ubiquitous pathogen-associated
64 molecular pattern (PAMP) recognized by the cellular machinery, which can arise as a
65 replication intermediate for viruses with an RNA genome, or from convergent transcription for
66 DNA viruses (6). In mammals, dsRNA recognition is driven by specific receptors including the
67 cytoplasmic RIG-Like Receptors (RLRs) and endosomal Toll Like Receptors (TLRs) (7).
68 Sensing of dsRNA by these receptors results in the activation of a complex signaling cascade
69 leading to the production of type I interferon (IFN), which in turn triggers the expression of
70 IFN stimulated genes (ISG) and the establishment of the antiviral state (8). The ultimate
71 outcome of this vertebrate-specific antiviral response is translation arrest and cell death by
72 apoptosis (9).

73 The revolution brought by the discovery of the CRISPR-Cas9 technology has provided
74 biologists with an invaluable tool to edit the genome at will and easily perform individual gene
75 knock-out (10). This technique is perfectly suited to perform genome-wide screens in a
76 relatively fast and easy to implement manner, especially when the readout is based on cell
77 survival. For this reason, numerous CRISPR-Cas9 loss of function screens have been performed
78 based on cell survival after infection with different viruses (11–13). These approaches allowed
79 the identification of novel virus-specific as well as common factors involved in antiviral defense
80 mechanisms or in cellular permissivity to virus infection.
81 Here, we chose to take advantage of the fact that dsRNA is almost always detected in virus-
82 infected cells (6) and is a potent inducer of apoptosis to design a genome-wide screen aiming
83 at identifying host genes that when edited resulted in increased cell survival to dsRNA and viral
84 challenge. To this aim, we performed a CRISPR-Cas9 screen based on cell survival in HCT116
85 cells after either cationic lipid-based transfection of an *in vitro* transcribed long dsRNA or
86 infection with the model alphavirus SINV, which replicates *via* a dsRNA intermediate.
87 Our results indicate that genes involved in limiting attachment and therefore entry, be it of the
88 synthetic dsRNA or SINV, are vastly over-represented after selection. We validated two genes
89 of the heparan sulfate pathway (namely *SLC35B2* and *B4GALT7*) as required for dsRNA
90 transfectability and SINV infectivity. We also identified and characterized COG4, a component
91 of the Conserved Oligomeric Golgi (COG) complex, as a novel factor involved in susceptibility
92 to dsRNA and viral induced cell death linked to the heparan sulfate biogenesis pathway.
93
94 **Results**
95 **Genome-wide CRISPR/Cas9 screen based on cell survival upon dsRNA transfection**
96 **identify factors of the heparan sulfate pathway**
97 In order to identify cellular genes that are involved in the cellular response to dsRNA, which
98 culminates with cell death, we performed a CRISPR/Cas9 genome-wide loss-of-function screen

99 in the human colon carcinoma cell line HCT116. This cell line is highly suitable for
100 CRISPR/Cas9 genetic screening procedures (14) and can be easily infected with SINV with
101 visible cytopathic effects at 24 and 48 hours post infection (hpi) (Fig. S1A). Moreover,
102 transfection of an *in vitro* transcribed 231 bp-long dsRNA by a cationic lipid-based transfection
103 reagent in HCT116 cells led to strong cell death at 24 and 48 hours post treatment (hpt) (Fig.
104 S1B).
105 We generated a Cas9-expressing HCT116 monoclonal cell line (Fig. S1C) that we stably
106 transduced with the human genome-wide lentiviral Brunello library composed of 76 441
107 sgRNAs targeting 19 114 genes, as well as about 1000 non-targeting sgRNAs as controls (15).
108 We then applied a positive selection by lipofecting 30 million transduced cells per replicate
109 with the synthetic long dsRNA and we collected the surviving cells 48h later. In parallel, the
110 same initial amount of stably transduced cells was left untreated as control (Input) for each
111 replicate (Fig. 1A). DNA libraries from the input samples were generated, sequenced and
112 quality checked. In particular, we verified the sgRNA coverage by observing the presence of
113 the 4 guides per genes for 18 960 genes (99.2% of the genes) and 3 sgRNAs per gene for the
114 remaining 154 genes (0.2% of the genes) (Dataset S1).
115 Using the MAGeCK software (16), we assessed the normalized read count distribution of the
116 control and dsRNA-treated biological triplicates, which, despite a quite homogenous sgRNA
117 distribution, showed the presence of few outliers upon selection (Fig. 1B). We identified eight
118 genes that were significantly enriched with a false discovery rate lower than 1% (FDR1%).
119 Among those, four genes belonged to the heparan sulfate biosynthesis pathway (namely,
120 *SLC35B2*, *B4GALT7*, *EXT1* and *EXT2*) and three were components of the conserved oligomeric
121 golgi complex (namely *COG3*, *COG4* and *COG8*) (Fig. 1C, Dataset S2). In particular, all four
122 sgRNAs targeting each of *SLC35B2*, *B4GALT7, COG4* genes were enriched upon dsRNA
123 selection (Fig. S1D).

124 Heparan sulfate (HS) is a linear polysaccharide that is covalently attached to core proteins in
125 proteoglycans (PG) on the cell surface (for review, see ref. (17)). Among many properties, HS
126 plays a role in binding of protein ligands and as a carrier for lipases, chemokines and growth
127 factors (17, 18), but also as a viral receptor (19). HS biosynthesis takes place in the Golgi, where
128 most of the biosynthetic enzymes are anchored to the Golgi membrane (20).
129 We first validated the resistance phenotype to dsRNA of *SLC35B2* and *B4GALT7*, the two top
130 hits identified in the screen (Fig. 1C, Fig. S1D), by generating two individual knock-out clones
131 for each gene by CRISPR-Cas9 editing in HCT116cas9 cells (Fig. S2). Knock-out of either
132 *SLC35B2* or *B4GALT7* genes abolished cell death induced by dsRNA lipofection compared to
133 parental HCT116cas9 cells, as assessed by the measurement of cell viability 48h post
134 transfection (Fig. 1D, left part of the graph). These results demonstrated the involvement of
135 SLC35B2 and B4GALT7 in dsRNA-induced cell death.
136 The observed resistance to dsRNA in the mutants could occur at many different steps: dsRNA
137 liposome attachment and entry, recognition, induction of the IFN pathway or apoptosis. To test
138 whether the first step was affected, we employed a nucleic acid delivery method that was not
139 based on cationic lipid transfection. In particular, we used nucleofection (an electroporation-
140 based transfection method) to introduce long dsRNAs into HCT116 cells and we showed that
141 this approach totally restored cell death in *SLC35B2* and *B4GALT7* knock-out cells (Fig. 1D,
142 right part of the graph). In addition, we also performed liposome-based transfection of an *in*
143 *vitro* transcribed Cy5-labelled dsRNA in *SLC35B2* and *B4GALT7* KO cells and assessed the
144 Cy5 fluorescence at 48 h post-transfection by FACS analysis (Fig. 1E-F). Although the number
145 of Cy5 positives (Cy5+) cells was not significantly different in the *B4GALT7* KO clones and
146 only slightly lower in the *SLC35B2* KO cells compared to WT cells (Fig. 1E), we observed a
147 significant reduction of at least 80% of the median Cy5 fluoresence in both *B4GALT7* and

148 *SLC35B2* KO cells relative to control (Fig. 1F), thereby indicating a significant drop in the
149 number of transfected Cy5-labeled RNA molecules per cells.
150 We also confirmed that liposome-based transfection of nucleic acid such as plasmidic DNA
151 was impaired in *SLC35B2* and *B4GALT7* KO cells, by transfecting a GFP-expressing plasmid
152 using Lipofectamine 2000 in wild type or knock-out cells (Fig. S3A, left panels and Fig. S3B).
153 Nonetheless, GFP expression could be restored in all cell lines upon nucleofection (Fig. S3A,
154 right panels).
155 To establish whether impairment of the HS synthesis is directly linked to a defect in dsRNA
156 entry and increased cell survival, we measured the extracellular HS levels in *SLC35B2* and
157 *B4GALT7* KO cells. We measured a substantial reduction of the extracellular HS staining as
158 assessed by FACS measurement of two independent *SLC35B2* and *B4GALT7* KO clones
159 compared to HCT116 wild type cells (Fig. 1G). To confirm the importance of HS at the cell
160 surface for liposome-based transfection, we mimicked the HS-defective phenotype by
161 removing extracellular HS in parental HCT116cas9 cells either enzymatically (with heparinase)
162 or chemically (with sodium chlorate NaClO3) (Fig. S3C-D). We tested the transfectability of a
163 GFP-expressing plasmid by measuring either the relative number of GFP positive cells or the
164 relative median of GFP intensity of fluorescence by FACS analysis. Although the relative
165 number of GFP positive cells was not significantly reduced by heparinase treatment (Fig. S3C),
166 it caused a reduction in GFP intensity in HCT116cas9 treated cells, thereby recapitulating the
167 GFP plasmid lipofection defect observed in *SLC35B2* and *B4GALT7* KO (Fig. S3D). Moreover,
168 this effect correlates with the reduction of extracellular HS by enzymatic treatment quantified
169 by FACS (Fig. S3E), which demonstrates that extracellular HS are crucial for transfection by
170 lipofection. In the case of NaClO3 treatment, despite the reduction in both the relative number
171 of GFP positive cells (Fig. S3C) and the relative median of GFP intensity of fluorescence(Fig.
172 S3D) compared to control, we could not observe a correlation with a decrease in overall

173 extracellular HS (Fig. S3E). This could be due to the fact that while a mix of heparinase I & III
174 remove every kind of extracellular heparan sulfates, NaClO3 only impairs the O-sulfation (21).
175 Taken together, our results show that knocking out *SLC35B2* and *B4GALT7* results in reduced
176 levels of extracellular HS, which in turn impairs liposome-based transfectability of HCT116
177 cells. Moreover, the validation of these two top hits indicates that other candidates might be
178 suitable for further analysis and may also have an impact on the dsRNA resistance phenotype.
179

180 **COG4 is involved in dsRNA-induced cell death partly via the heparan sulfate pathway**

181 Among the significant hits of our genome-wide screen were proteins related to COG complex,
182 namely COG4, COG3 and COG8. The COG complex is a hetero-octameric complex containing
183 8 subunits (COG1-8) interacting with numerous proteins mainly involved in intra-Golgi
184 membrane trafficking such as vesicular coats, Rab proteins and proteins involved in SNARE
185 complex (22, 23). This interaction with the trafficking machinery is crucial for the proper
186 functionality of the Golgi apparatus and mutations in the COG complex result in severe cellular
187 problems such as glycosylation defect (24–27), which are due to mislocalization of recycling
188 Golgi enzymes (28, 29).
189 Since we retrieved three out of the eight COG family members in our CRISPR/Cas9 screen
190 suggesting their importance in dsRNA-induced cell death, we tested the effect of their
191 inactivation by CRISPR-Cas9. *COG4* being the most enriched COG gene in our screen, we
192 generated a polyclonal *COG4* KO HCT116cas9 cell line and validated their dsRNA resistance
193 phenotype resulting in an increase survival in response to synthetic dsRNA transfection (Fig.
194 S4A). We also observed a reduction in the relative number of Cy5 positives (Cy5+) cells and
195 the median Cy5 fluorescence in *COG4* KO cells relative to control by FACS analysis (Fig.
196 S4B-C).

197 To further confirm the involvement of the COG complex, we also tested the effect of dsRNA
198 transfection in previously generated HEK293T KO *COG3*, 4 and 8 cells (Fig. 2A) (30).
199 Interestingly, while *COG8* mutants did not display a significant survival phenotype in response
200 to dsRNA lipofection, *COG3* and *COG4* KO HEK293 cells did. In addition, the survival
201 phenotype could be complemented by stable expression of a COG4-GFP construct compared
202 to *COG4* KO cells (Fig. 2A). Moreover, although we could not detect a decrease in the relative
203 number of Cy5 positives (Cy5+) cells in *COG4* KO cells relative to the controls (Fig. 2B), the
204 median Cy5 fluorescence in *COG4* KO cells was significantly reduced compared to both
205 HEK293T and COG4 rescued cells (Fig. 2C), thereby indicating a significant decrease in the
206 number of transfected Cy5-labeled RNA molecules per cells.
207 In agreement, dsRNA accumulation appeared to be significantly reduced, but still present, in
208 HEK293T *COG4* KO cells compared to control cells as determined by RT-qPCR analysis of
209 dsRNA isolated from cells 24h after transfection (Fig 2D) and this correlated with reduced IFN-
210 beta accumulation in HEK293T KO *COG4* cells compared to control cells (Fig. 2E).
211 These results indicated that dsRNA transfectability was strongly reduced but not totally
212 impaired in the absence of COG4 and that dsRNA could be still detected in *COG4* KO cells in
213 order to activate type-I IFN response.
214 We confirmed the reduced internalization of dsRNA in COG4 mutant cells by transfecting
215 rhodamine-labeled poly(I:C), a synthetic dsRNA analog, in HEK293T *COG4* KO or WT cells
216 (Fig. 2F) and by counting the number of poly I:C foci per cell at 6, 12 and 24 h post transfection
217 (Fig. 2G). We could observe a significant reduction in rhodamine positive foci in HEK293T
218 *COG4* KO during the time course, suggesting a defect in dsRNA internalization, which could
219 explain the increased survival phenotype.
220 In order to assess whether the *COG4* KO survival phenotype was associated with a defect in
221 the heparan sulfate pathway, we stained extracellular HS and measured the HS expression by

222 FACS analysis. We observed a decrease of extracellular HS in KO *COG4* cells compared to
223 control cells (WT and rescued), which demonstrated that the COG complex is related to the HS
224 biosynthesis pathway (Fig. S4D)
225 The reduction in extracellular HS could correlate with a decrease in transfectability and explain
226 the survival phenotype in KO *COG4* cells. Surprisingly however, lipofection of a GFP
227 expressing plasmid indicated that HEK293T *COG4* KO cells are still transfectable with a
228 plasmid DNA compared to control cells as observed by FACS analysis (Fig. S4E-F).
229 Altogether these findings indicate that the COG complex is involved in HS biosynthesis and
230 that removal of *COG4* results in a lower accumulation of HS at the cell surface, which most
231 likely translates in a reduced transfectability of dsRNA. However, as opposed to the
232 observations in *SLC35B2* or *B4GALT7* KO cells, the cells are still transfectable with a plasmid
233 DNA and, although to a lower extent, with dsRNA. Interestingly, the increased cell survival
234 phenotype of *COG4* KO cells upon dsRNA transfection does correlate with a reduced, but still
235 measurable, IFN- β production.
236
237 **Cell survival based genome-wide CRISPR/Cas9 screen identifies *COG4* as a permissivity**
238 **factor to SINV**
239 SINV is a small enveloped virus with a single stranded RNA genome of positive polarity. The
240 virus belongs to the *Togaviridae* family, alphavirus genus and is considered as the model for
241 other medically important viruses such as chikungunya virus (CHIKV) and Semliki forest virus
242 (SFV). During its infectious cycle, SINV produces dsRNA as a replication intermediate and
243 induces cytopathic effects in mammalian cells, leading to cell death within 24 to 48 h post-
244 infection (31).
245 In order to identify host genes that are related to SINV-induced cell death and infection, we
246 performed a CRISPR/Cas9 knock-out screen in HCT116cas9 cells, which are susceptible to

247 this virus (Fig. 3A, Fig. S1). After transduction with the CRISPR lentiviral genome-wide
248 knockout library, puromycin-resistant HCT116 cells were infected with SINV-GFP at a MOI
249 of 0.1 and selected for cell survival. Using the MAGeCK software (16), we assessed the
250 normalized read count distribution of the control and SINV-infected biological triplicates,
251 which, despite a quite homogenous sgRNA distribution, showed the presence of few outliers
252 upon selection (Fig. 3B). We identified two genes that were significantly enriched with a false
253 discovery rate lower than 25% (FDR25%), notably *SLC35B2* and *B4GALT7* (Dataset S3, Fig.
254 3C). Genes of the heparan sulfate pathway have been previously found in genome-wide
255 CRISPR-Cas9 loss of function studies looking for factors involved in the accumulation of
256 viruses such as Influenza, Zika and chikungunya virus (11, 32, 33). Interestingly, among the
257 top-ranking hits, we retrieved *COG4*, which was not previously associated with SINV infection
258 (Fig. 3C).
259 To validate the involvement of *COG4* during SINV infection, we infected HEK293T, *COG4*
260 KO or COG4 KO rescued HEK293T cells with SINV and measured cell viability at 24, 48 and
261 72 hpi. The cell viability assay revealed that the *COG4* KO cells were less sensitive at early
262 times points of SINV infection (24 & 48 hpi), but this tendency disappeared at 72 hpi (Fig. 3D.
263 In agreement, the determination of viral titer by plaque assay showed that *COG4* KO HEK293T
264 cells produced significantly less infectious viral particles than HEK293T or *COG4*-rescued
265 cells at 24 hpi but not at 48 hpi, underlining a possible delay in the infection and virus-induced
266 cell death (Fig. 3E). We also observed that GFP accumulated to lower levels in *COG4* KO than
267 in WT cells both at 24 and 48 h post-infection (hpi) (Fig. S5A). Finally, we noticed that the
268 reduced viral production in *COG4* KO cells was associated with a reduced accumulation of
269 viral dsRNA in the cytoplasm, when we infected WT or *COG4* KO cells with SINV-GFP and
270 performed immunostaining with the anti-dsRNA J2 antibody 24 hpi (Fig. S5B). Overall, our

271 results indicate that COG4 expression is needed for an efficient SINV infection and that its
272 absence can delay the infection thereby increasing cell survival in *COG4* KO cells.
273
274 **Discussion**

275 Several CRISPR/Cas9 screens aiming at identifying factors required for infection by specific
276 viruses have been described in the literature, but to our knowledge, none has been designed to
277 look at the effect of the only common factor between all those viruses, *i.e.* dsRNA. Here, we
278 used the Brunello sgRNA lentiviral library to screen for genes involved in HCT116 cells
279 survival to synthetic dsRNA transfection and to SINV infection. This allowed us to identify
280 components of the heparan sulfate biosynthesis pathway and of the COG complex as critical
281 host factors in the cellular response to above mentioned challenges. It has been already reported
282 that cell-survival-based CRISPR screens for viral host factors are biased toward genes linked
283 to the initial steps of the infection, and even more so to viral entry (11, 34). Thus, in our case,
284 HS is a well-known factor required for SINV entry due to the virus adaptation to cell culture
285 (35). We also retrieved genes of the HS pathway in our dsRNA-based screen, and we confirmed
286 the importance of extracellular HS for dsRNA-induced toxicity. This is mostly due to a decrease
287 of transfectability of the cells when HS are missing, which is linked to the fact that the
288 polyplexes used for transfection are positively charged and can interact electrostatically with
289 glycosaminoglycans (36, 37). Our work also points out to the limitations of survival-based
290 CRISPR-Cas9 screens. Thus in this study the selection pressure was too strong to allow the
291 identification of genes intervening after the entry step, thereby making the screen less sensitive.
292 Optimizing the selection procedure, *e.g.* by adjusting the concentration of dsRNA, or the
293 duration of treatment, may have allowed the identification of hits not solely implicated in the
294 transfection, but at the expense of specificity. Alternatively, new strategies should be designed
295 to overcome this problem, such as using fluorescent-based cell sorting in order to be less
296 stringent in the selection.

297 In addition to the HS pathway, we identified members of the COG complex, and more
298 specifically *COG4*, as factors involved in dsRNA transfection and SINV infection. Loss of
299 function COG4 mutant cells show a dsRNA-resistant phenotype as well as a reduction in
300 extracellular HS expression, similar to previously published reports for other COG proteins (33,
301 38). Surprisingly, even if the removal of COG4 expression results in a defect in the HS pathway,
302 we were still able to transfect the KO *COG4* cell line either with a plasmid encoding GFP or,
303 although to a lesser extent, dsRNA. In addition, the dsRNA molecules that are able to enter into
304 *COG4* KO HEK293T cells are still sufficient to induce the IFN-β mRNA production indicating
305 that the innate immune response is still functional in these mutant background. Nonetheless,
306 cell death induced by dsRNA appears to be lower in *COG4* KO cells, most likely due to a delay
307 in the infection.
308 Future work will be needed in order to assess whether this phenotype upon SINV infection is
309 only correlated with a defect in HS biogenesis in *COG4* mutants or to other function of COG4.
310 The fact that *COG4* KO cells seem to better survive to both synthetic dsRNA transfection and
311 viral infection opens several interesting perspectives. Indeed, since the COG complex is related
312 to glycosylation and membrane trafficking (23, 25, 39, 40), deficiency in one or more of its
313 components could potentially lead to a glycosylation and/or subcellular localization defect of
314 components of the innate immune response or of the apoptosis pathway, although this
315 possibility remains to be formally proven. The difference of transfectability of plasmid DNA
316 and dsRNA in *COG4* KO cells is also intriguing and could indicate that different kinds of
317 nucleic acids do not necessarily use the exact same routes to enter the cells upon liposome-
318 based transfection. Finally, there could be other defects linked to COG deficiencies(39, 41) that
319 could account for our observations and elucidating those will require further work. It is
320 particularly interesting that *COG3* and *COG4* knock-out cells display a dsRNA-induced cell

321 death resistance phenotype, while *COG8* mutants do not. This implies that only part of the COG
322 complex is involved in dsRNA uptake.
323 In conclusion, our work uncovered *COG4* as a new player in the HS production, which is
324 required for both SINV infection and dsRNA transfection. These results also highlight that
325 synthetic dsRNA is a powerful tool to identify novel key pathways of the cellular response to
326 RNA viruses.
327

328 **Materials and Methods**

329 **Cell culture and virus**

330 HCT116, HEK293T, HEK293T COG KOs, BHK21 and Vero R cells were maintained in
331 Dulbecco's Modified Eagle Medium (DMEM) 4.5 g/L glucose (Gibco, Thermo Fisher
332 Scientific Inc.) supplemented with 10% fetal bovine serum (FBS) (Takara) in a humidified
333 atmosphere of 5% CO_2 at 37°C. HEK293T *COG3*, *COG8* and *COG4* KO and *COG4* KO stably
334 rescued with COG4-GFP were described previously (42, 43). HCT116cas9 and HEK293T
335 COG4rescued were maintained in the same medium with addition of 10 μg/mL blasticidine.
336 HCT116 KO clones (*COG4*, *SLC35B2*#1 and #2, *B4GALT7*#1 and #2 were maintained in the
337 same medium with addition of 10 μg/mL blasticdine and 1 μg/mL puromycine.
338 SINV wild type (SINV) or expressing the green fluorescent protein (SINV-GFP) were produced
339 as previously decribed (44) in BHK21 cells. In the later, the promoter of SINV subgenomic
340 RNA was duplicated and inserted at the 3' extremity of the viral genome, the GFP sequence
341 was then inserted after this new promoter. Cells were infected with either SINV WT or SINV
342 GFP at a MOI of 10^{-1} and samples were harvested at 24 or 48 hours post-infection (hpi).
343

344 **Standard plaque assay**

345 10-fold dilutions of the viral supernatant were prepared. 50 μl aliquots were inoculated onto
346 Vero R cell monolayers in 96-well plates for 1 hour. Afterwards, the inoculum was removed
347 and cells were cultured in 2.5% carboxymethyl cellulose for 72 h at 37ºC in a humidified
348 atmosphere of 5% CO_2. Plaques were counted manually under the microscope. For plaque
349 visualization, the medium was removed, cells were fixed with 4% formaldehyde for 20 min and
350 stained with 1x crystal violet solution (2% crystal violet (Sigma-Aldrich), 20% ethanol, 4%
351 formaldehyde).
352
353 **J2 immunostaining**
354 HEK293T or KO *COG4* HEK293T cells were plated on millicell EZ slide (Millipore) and were
355 infected with SINV at an MOI of 0.1 for 24h. Cells were fixed with 4% formaldehyde diluted
356 in PBS 1x for 10 min at room temperature, followed by incubation in blocking buffer (0.2%
357 Tween X-100; PBS 1x; 5% normal goat serum) for 1 h. J2 antibody (Scicons) diluted in
358 blocking buffer at 1:1000 was incubated over night at 4°C. Between each steps, cells were
359 washed with PBS 1X-Tween 0.2%. Secondary antibody goat anti-mouse Alexa 594
360 (ThermoFisher) diluted at 1:1000 in PBS 1x-Tween 0.2% were incubated for 1 h at room
361 temperature. After DAPI staining (1:5000 dilution in PBS 1x for 5 min), slides were mounted
362 with a coverslip over anti-fading medium and observed by epifluorescence microscopy using
363 the BX51 (Olympus) microscope with a X 40 objective.
364
365 **Generation of HCT116cas9 line**
366 The HCT116cas9 cells, expressing human codon-optimized S. pyogenes Cas9 protein, were
367 obtained by transducing wild type HCT116 colorectal carcinoma cell line (ATCC® CCL-
368 247™) with lentiCas9-Blast lentiviral vector (Addgene #52962). Briefly, wild-type HCT116
369 cells were cultured in standard DMEM (GIBCO) medium supplemented with 10% Fetal bovine

370 serum (FBS, Gibco) and 100 U/mL of penicillin-Streptomycin (Gibco) at 37°C in 5% CO_2. The
371 cells were transduced at 80% confluency in a 10 cm tissue culture plate, using 6 mL lentiviral
372 supernatant supplemented with 4μg/mL of polybrene (H9268, sigma) for 6 hours. The
373 transduction medium was replaced with fresh growing medium for 24h before starting the
374 selection. Transduced HCT116cas9 cells were selected for 10 days and maintained in growing
375 medium supplemented with 10μL/mL of Blasticidin (Invivogen).
376
377 **High titer lentiviral sgRNA library production**
378 The production of high titer Human sgRNA Brunello lentiviral library which contains 4 sgRNA
379 per gene (15) (Addgene #73178), was performed by transfecting HEK293T cells in five 15 cm
380 tissue culture plates using PEI (Polyethylenimin Linear, MW 25,000, 23966-1-A, Polysciences)
381 transfection method (45). Briefly, for each 15 cm plate containing 20 mL of medium, 10μg of
382 sgRNA library, 8μg of psPAX2 and 2μg of pVSV diluted in 500μL of NaCl 150 mM were
383 combined with 40μL of PEI (1.25 mg/mL) dissolved in 500μL of NaCl 150 mM. The mix was
384 incubated 30 minutes at room temperature and the formed complexes were added dropwise on
385 the cells. After 6 hours, the medium was replaced and the viral supernatant was collected after
386 48 hours and after 72 hours. The supernatant was filtered through a 0.45μm PES filter and the
387 viral particles concentrated 100 times using Lenti-X™ Concentrator (Takara) before storage at
388 -80. The viral titer was established by counting puromycin resistant colonies formed after
389 transducing HCT116 cells with serial dilutions of viral stock. HCT116cas9 cells were
390 transduced with lentivirus-packaged Brunello sgRNA library at a MOI of 0.3. The lentiviral
391 library has been sequenced to verify that all the lenti-sgRNA are represented.
392
393 **Genome-wide CRISPR/Cas9 knock-out screens**

394 For each replicate (n=3), $5x10^6$ stably transduced cells/dish were seeded in $6x15cm^2$ plate in
395 order to keep a 300X representativity of the sgRNA library. Untreated samples (Input) were
396 collected as controls. One day later, cells were either lipofected with 1 μg/mL dsRNA-Citrine
397 or infected with SINV at MOI of 0.1 and cultured at 37°C 5% CO_2. Cells were washed with
398 PBS 1X 48 hours post treatment, to remove dead cells and fresh media was added to surviving
399 clones. Cells were expanded and all cells were collected 6 days post dsRNA transfection and
400 18 days post SINV infection.
401 Genomic DNA was isolated by resuspending the cell pellet in 5 mL of resuspension buffer (50
402 mM Tris-HCl pH 8.0, 10 mM EDTA, 100 µg/ml RNaseA), 0.25 mL of 10% SDS was added
403 and incubated 10 mins at RT after mix. After incubation, the sample was sonicated and
404 incubated 30 mins at RT with 10 uL of proteinase K (10mg/mL). 5 mL of
405 Phenol/Chloroform/Isoamyl Alcohol solution was added and followed by a spin down 60 mins
406 at 12000g/20°C. Upper phase was transferred into a new tube and 500uL of NaAc 3M and 5
407 mL of isopropanol was added then incubation over night at RT and followed by a centrifuge 30
408 mins/20°C/12000g. Pellet was washed using EtOH and dissolve in H2O.
409 Illumina P5 and P7-barcoded adaptors were added by PCR on gDNA samples according to the
410 GoTaq protocol (Promega). PCR amplicons were gel purified and sequenced on a HiSeq4000
411 (Illumina) to obtain about 30 million reads for each samples. Enrichment of sgRNAs was
412 analysed using MaGeCK with default parameters (16). Primers used to generate the PCR
413 products are listed in Table S1. The results of the dsRNA and SINV screen are available in
414 Dataset S1 and S2, respectively
415
416 **Generation of monoclonal SLC35B2 and B4GALT7 and polyclonal COG4 knock-out**
417 **HCT116 cell lines**

418 The sgRNA expression vectors targeting either SLC35B2, B4GALT7 or COG4 (sgRNA
419 sequences selected were the 2 most enriched sgRNA from the Brunello library in the dsRNA
420 screen) genes were produced by annealing the "sense" and "antisense" oligonucleotides (Table
421 S1) at a concentration of 10 μM in 10 mM Tris-HCl (pH 8.0), 50 mM MgCl2 in 100 μL. The
422 mixture was incubated at 95 °C for 5 minutes and then allowed to cool down to room
423 temperature. The oligonucleotide duplex thus formed was cloned into the BbsI restriction site
424 of the plasmid pKLV-U6gRNA (BbsI)-pGKpuro2ABFP (Addgene#62348). The lentiviral
425 supernatant from single transfer vector was produced by transfecting HEK293T cells (ATCC®
426 CRL-3216™) with the transfer vector, psPAX2 packaging plasmid (Addgene #12260) and the
427 pVSV envelope plasmid (Addgene #8454) in proportion 5:4:1 using Lipofectamine™ 2000
428 (Themofisher) reagent according to manufacturer protocol. Standard DMEM (GIBCO) medium
429 supplemented with 10% Fetal bovine serum (FBS, Gibco) and 100 U/mL of penicillin-
430 Streptomycin (Gibco) was used for growing HEK293T cells and for lentivirus production. One
431 10 cm plate of HEK293T cells at 70-80% confluency was used for the transfection. The medium
432 was replaced 8 hours post-transfection. After 48 hours the medium containing viral particles
433 was collected and filtered through a 0.45μm PES filter. The supernatant was directly used for
434 transfection or stored at -80°C. A 6-well plate of HCT116cas9 cells at 80% confluency was
435 transduced using 600 μL of lentiviral supernatant (300 μL of each lentivirus produced for each
436 duplexes) supplemented with 4 μg/mL polybrene (Sigma) for 6 hours. The transduction media
437 was then changed with fresh DMEM for 24 hours then the transduced cells were selected using
438 DMEM containing 10 μg/mL Blasticidin (Invivogen) and 1 μg/mL Puromycin (Invivogen).
439 Genomic DNA was isolated from individual colonies and KO clones were screened by PCR
440 (primers in Table S1). The expected WT band for SLC35B2 is 469 bp and the mutant band 132
441 bp. For B4GALT7, the WT band is 341 bp and mutant band 180 bp. For laboratory purposes,

442 the SLC35B2 clones have been generated into HCT116cas9 cells that are expressing mCherry
443 and Citrine due to integration of miReporter-PGK (Addgene#82477).
444
445 **Nucleic acids delivery**
446 Transfection using lipofectamine2000 (InvitroGen – 11668019) were performed following
447 manufacturer's instructions. For nucleofection, cells were nucleofected using Nucleofector SE
448 solution and reagent into Nucleocuvette following manufacturer's instructions using 4D-
449 Nucleofector System (Lonza). The cell number and nucleic acid amounts are indicated in each
450 figure legends. P-EGFP-N1 (Addgene plasmid#2491) was used in transfection and
451 nucleofection experiments as a control.
452
453 **Viability assay**
454 PrestoBlue (PB) reagent (ThermoFisher – A13261) was used for viability assay according to
455 the manufacturer's protocol. After 24 to 48 hours post treatment (SINV, dsRNA
456 transfection/nucleofection), cells were incubated with PB reagent and cell viability was
457 assessed by measuring the fluorescence (excitation 570 nm; emission 590 nm) after 20 mins
458 incubation using SAFAS spectrofluorometer (Xenius XC). Cell viability was expressed as a
459 percentage relative to untreated cells.
460
461 **Heparinase & sodium chlorate treatment and heparan sulfate staining**
462 Heparinase: 1.10^6 were treated with 2U of Heparinase I and III blend from *Flavobacterium*
463 *heparinum* (Merck – H3917) for 1 h at 37°C 5% CO2 in DMEM and then cells were reverse
464 transfected with 2 µg of GFP using lipofectamine2000 (Invitrogen) in 6 well plate.

465 Sodium chlorate: HCT116cas9 cells grow in 50 mM sodium chlorate (Merck – 1.06420)
466 DMEM 10 % FBS for at least 48 h then 150 000 cells were reverse transfected with 500 ng of
467 GFP using lipofectamine 2000 (Invitrogen) in 24 well plate.
468 24 (heparinase) or 48 (sodium chlorate) hours post treatment, cells were detach using PBS
469 0.02% EDTA, then heparan sulfate was stained using 1:30 of F58-10E4 as primary antibody
470 (AMSBIO, cat#370255-S) in PBS 3% BSA for 30 to 40 minutes on ice then washed with PBS
471 1% FBS and incubated with 1:30 anti-mouse Alexa Fluor 594 (Thermo, A-11032) in PBS 3%
472 BSA, washed twice using PBS 1% FBS then and analysed on a FACSCalibur flow cytometer.
473
474 **dsRNA preparation**
475 PCR fragments corresponding to 231 nts of the Citrine coding sequence were amplified from
476 ES-FUCCI plasmid (Addgene plasmid#62451) using primers containing T7 promoter sequence
477 with 2 distinct PCR fragment allowing the positive-sense or negative-sense RNA. Primers used
478 to generate the PCR products are listed in Table S1. The PCR fragments were produced using
479 DyNAzyme EXT DNA Polymerase (F-505S - Thermo Scientific) and purified using Monarch
480 DNA extraction (T1020L - New England Biolab). In vitro transcription (IVT) with homemade
481 T7 RNA polymerase was performed for 4 hours at 37°C. To label the IVT RNA, 1/10th of Cy5-
482 CTP (Amersham CyDye Fluorescent Nucleotides Cy5-CTP, GE Healthcare Life sciences) was
483 included in the IVT reaction. IVT RNA was digested with DNase I (EN0525 - Thermo
484 Scientific) for 30 min at 37°C and IVT product was purified, unincorporated nucleotides
485 removed and size checked using UV shadow (8% acrylamide-urea gel) followed by phenol-
486 chloroform extraction and nanodrop quantification for each strand. We then mix an equal
487 quantity of positive-strand and negative-strand RNA, heat for 5' at 95°C followed by slow cool
488 down to RT. The integrity of dsRNA is then checked by RNases T1 (EN0541 - Thermo
489 Scientific) and V1 (AM2275, Ambion) digestion.

490 **Microscopy**

491 Imaging of cells treated with dsRNA/GFP plasmid was carried out on the Observer A1 (Zeiss)
492 microscope and analyzed using Fiji (46). Images of cells transfected with Poly(I:C) (LMW)
493 Rhodamine (tlrl-piwr – Invivogen)(1,8 μg/mL, 24h post plating of 76 000 cells) into Lab-Tek
494 on glass coverslip (155411- Thermo Scientific) were acquired using a 100x Plan Apochromat
495 oil immersion NA1.4 objective on a spinning disk system Axio Observer Z1 (Zeiss) every 20
496 minutes for 72 hours. All pictures were acquired under the same conditions (laser power and
497 amplification gain) then processed with Fiji. Images of cells infected with SINV stained with
498 J2 antibody were carried out on BX51 microscope (Olympus).

499

500 **FACS analysis**

501 The cells intended for analysis by flow cytometry are recovered mechanically (PBS 0.5 mM
502 EDTA) or using trypsin, washed in PBS and then suspended in PBS 1 % FBS. Each acquisition
503 includes at least 10,000 events and is performed on the FACScalibur (BD Bioscience) device.
504 The data produced is processed using FlowJo software (FlowJo LLC).

505

506 **RT-qPCR analysis**

507 Total RNA was isolated using TRIzol (Invitrogen - 15596026) following manufacturer's
508 instructions. 1 µg of RNA was reverse transcribed using SuperScript IV Vilo (Invitrogen –
509 11756050) according to manufacturer's instructions. Real-time PCR was performed using
510 SYBR Green (Applied Biosystem – 4309155) and primers listed in Table S1 at an annealing
511 temperature of 60°C on a CFX96 thermal cycler (Biorad). Generated data were analysed using
512 the CFX Manager Software (Biorad).

513

514 **Western blot analysis**

515 Proteins were extracted using RIPA lysis buffer. Proteins were quantified by the Bradford
516 method and 20 to 30 µg of total protein extract was loaded on 4-20% Mini-PROTEAN®
517 TGX™ Precast Gels (Biorad). After transfer onto nitrocellulose membrane, equal loading was
518 verified by Ponceau staining. Membranes were blocked in 5% milk and probed with the
519 following antibodies: anti-Flag M2 (SIGMA, #F1804) and anti-GAPDH (clone 6C5, BioRad #
520 MCA4739P). Detection was performed using Chemiluminescent Substrate (Thermo Fisher).
521

522 **Data availability**

523 The CRISPR-Cas9 screen sequencing data discussed in this manuscript has been deposited on
524 NCBI's Sequence Read Archive (SRA) and has been attributed the BioProject ID
525 PRJNA662202. It can be accessed at the following URL:
526 https://submit.ncbi.nlm.nih.gov/subs/bioproject/SUB8109948/overview
527

528 **Acknowledgments**

529 The authors would like to thank members of the Pfeffer laboratory for discussion, Delphine
530 Richer for technical help, Dr. Jean-Daniel Fauny for help with the spinning disk microscope
531 and Dr. Frédéric Gros for help with FACS analysis, Dr Carla Saleh for providing us the SINV
532 WT and GFP clones.
533 This work was funded by the European Research Council (ERC-CoG-647455 RegulRNA) and
534 was performed under the framework of the LABEX: ANR-10-LABX-0036_NETRNA, which
535 benefits from a funding from the state managed by the French National Research Agency as
536 part of the Investments for the future program. This work has also received funding from the
537 People Programme (Marie Curie Actions) of the European Union's Seventh Framework
538 Program (FP7/2007-2013) under REA grant agreement n° PCOFUND-GA-2013-609102,
539 through the PRESTIGE program coordinated by Campus France (to EG), and from the French

540 Minister for Higher Education, Research and Innovation (PhD contract to OP). VL was
541 supported by the National Institutes of Health (R01GM083144). Sequencing was performed by
542 the GenomEast platform, a member of the 'France Génomique' consortium (ANR-10-INBS-
543 0009).
544

545 **Authors contribution**

546 SP and EG conceived the project. SP, EG and OP designed the work and analysed the results.
547 OP, EG, and RPN performed the experiments. EG and OP set up the CRISPR/Cas9 screens,
548 RPN generated the lentivirus library and the HCT16-Cas9 cell line. OP and RPN performed the
549 bioinformatics analysis of the screens. OP generated the SLC35B2 and B4GALT7 KO clones.
550 OP generated IVT dsRNA and perform validation of cell survival. EG produced SINV-GFP
551 viral stock, performed the infections and analysed viral titers. OP performed FACS analyses.
552 EG and OP performed the immunofluorescence assays. OP analysed the live-imaging
553 microscopy data. VL provided the COG KO cells and antibodies. OP, EG and SP wrote the
554 manuscript with input from the other authors. SP and EG coordinated the work. SP assured
555 funding. All authors reviewed the final manuscript.
556

557 **References**

558 1. Bomsel M, Alfsen A. 2003. Entry of viruses through the epithelial barrier: pathogenic
559 trickery. Nat Rev Mol Cell Biol 4:57–68.
560 2. Rusnati M, Vicenzi E, Donalisio M, Oreste P, Landolfo S, Lembo D. 2009. Sulfated K5
561 Escherichia coli polysaccharide derivatives: A novel class of candidate antiviral
562 microbicides. Pharmacology & Therapeutics 123:310–322.
563 3. Byrnes AP, Griffin DE. 1998. Binding of Sindbis virus to cell surface heparan sulfate. J
564 Virol 72:7349–7356.
565 4. Smith TJ, Cheng RH, Olson NH, Peterson P, Chase E, Kuhn RJ, Baker TS. 1995. Putative
566 receptor binding sites on alphaviruses as visualized by cryoelectron microscopy. Proc Natl
567 Acad Sci USA 92:10648–10652.
568 5. Wahlberg JM, Bron R, Wilschut J, Garoff H. 1992. Membrane fusion of Semliki Forest
569 virus involves homotrimers of the fusion protein. J Virol 66:7309–7318.
570 6. Weber F, Wagner V, Rasmussen SB, Hartmann R, Paludan SR. 2006. Double-Stranded
571 RNA Is Produced by Positive-Strand RNA Viruses and DNA Viruses but Not in
572 Detectable Amounts by Negative-Strand RNA Viruses. J Virol 80:5059–5064.
573 7. Schlee M, Hartmann G. 2016. Discriminating self from non-self in nucleic acid sensing.
574 Nat Rev Immunol 16:566–580.
575 8. Stetson DB, Medzhitov R. 2006. Type I Interferons in Host Defense. Immunity 25:373–
576 381.
577 9. García MA, Meurs EF, Esteban M. 2007. The dsRNA protein kinase PKR: Virus and cell
578 control. Biochimie 89:799–811.
579 10. Shalem O, Sanjana NE, Zhang F. 2015. High-throughput functional genomics using
580 CRISPR-Cas9. Nat Rev Genet 16:299–311.
581 11. Han J, Perez JT, Chen C, Li Y, Benitez A, Kandasamy M, Lee Y, Andrade J, tenOever B,
582 Manicassamy B. 2018. Genome-wide CRISPR/Cas9 Screen Identifies Host Factors
583 Essential for Influenza Virus Replication. Cell Reports 23:596–607.
584 12. Park RJ, Wang T, Koundakjian D, Hultquist JF, Lamothe-Molina P, Monel B, Schumann
585 K, Yu H, Krupzcak KM, Garcia-Beltran W, Piechocka-Trocha A, Krogan NJ, Marson A,
586 Sabatini DM, Lander ES, Hacohen N, Walker BD. 2017. A genome-wide CRISPR screen
587 identifies a restricted set of HIV host dependency factors. Nat Genet 49:193–203.
588 13. Zhang R, Miner JJ, Gorman MJ, Rausch K, Ramage H, White JP, Zuiani A, Zhang P,
589 Fernandez E, Zhang Q, Dowd KA, Pierson TC, Cherry S, Diamond MS. 2016. A CRISPR

590 screen defines a signal peptide processing pathway required by flaviviruses. Nature
591 535:164–168.
592 14. Golden RJ, Chen B, Li T, Braun J, Manjunath H, Chen X, Wu J, Schmid V, Chang T-C,
593 Kopp F, Ramirez-Martinez A, Tagliabracci VS, Chen ZJ, Xie Y, Mendell JT. 2017. An
594 Argonaute phosphorylation cycle promotes microRNA-mediated silencing. Nature
595 542:197–202.
596 15. Doench JG, Fusi N, Sullender M, Hegde M, Vaimberg EW, Donovan KF, Smith I,
597 Tothova Z, Wilen C, Orchard R, Virgin HW, Listgarten J, Root DE. 2016. Optimized
598 sgRNA design to maximize activity and minimize off-target effects of CRISPR-Cas9. Nat
599 Biotechnol 34:184–191.
600 16. Li W, Xu H, Xiao T, Cong L, Love MI, Zhang F, Irizarry RA, Liu JS, Brown M, Liu XS.
601 2014. MAGeCK enables robust identification of essential genes from genome-scale
602 CRISPR/Cas9 knockout screens. Genome Biol 15:554.
603 17. Li J-P, Kusche-Gullberg M. 2016. Heparan Sulfate: Biosynthesis, Structure, and Function,
604 p. 215–273. *In* International Review of Cell and Molecular Biology. Elsevier.
605 18. Bishop JR, Schuksz M, Esko JD. 2007. Heparan sulfate proteoglycans fine-tune
606 mammalian physiology. Nature 446:1030–1037.
607 19. Cagno V, Tseligka ED, Jones ST, Tapparel C. 2019. Heparan Sulfate Proteoglycans and
608 Viral Attachment: True Receptors or Adaptation Bias? Viruses 11.
609 20. Lindahl U, Couchman J, Kimata K, Esko JD. 2015. Proteoglycans and Sulfated
610 Glycosaminoglycans, p. . *In* Varki, A, Cummings, RD, Esko, JD, Stanley, P, Hart, GW,
611 Aebi, M, Darvill, AG, Kinoshita, T, Packer, NH, Prestegard, JH, Schnaar, RL, Seeberger,
612 PH (eds.), Essentials of Glycobiology, 3rd ed. Cold Spring Harbor Laboratory Press, Cold
613 Spring Harbor (NY).
614 21. Safaiyan F, Kolset SO, Prydz K, Gottfridsson E, Lindahl U, Salmivirta M. 1999. Selective
615 Effects of Sodium Chlorate Treatment on the Sulfation of Heparan Sulfate. J Biol Chem
616 274:36267–36273.
617 22. Blackburn JB, D'Souza Z, Lupashin VV. 2019. Maintaining order: COG complex controls
618 Golgi trafficking, processing, and sorting. FEBS Lett 593:2466–2487.
619 23. Willett R, Ungar D, Lupashin V. 2013. The Golgi puppet master: COG complex at center
620 stage of membrane trafficking interactions. Histochem Cell Biol 140:271–283.
621 24. Kranz C, Ng BG, Sun L, Sharma V, Eklund EA, Miura Y, Ungar D, Lupashin V, Winkel
622 RD, Cipollo JF, Costello CE, Loh E, Hong W, Freeze HH. 2007. COG8 deficiency causes

623 new congenital disorder of glycosylation type IIh. Human Molecular Genetics 16:731–
624 741.
625 25. Reynders E, Foulquier F, Leão Teles E, Quelhas D, Morelle W, Rabouille C, Annaert W,
626 Matthijs G. 2009. Golgi function and dysfunction in the first COG4-deficient CDG type
627 II patient. Human Molecular Genetics 18:3244–3256.
628 26. Spaapen LJM, Bakker JA, van der Meer SB, Sijstermans HJ, Steet RA, Wevers RA,
629 Jaeken J. 2005. Clinical and biochemical presentation of siblings with COG-7 deficiency,
630 a lethal multiple O- and N-glycosylation disorder. J Inherit Metab Dis 28:707–714.
631 27. Zeevaert R, Foulquier F, Jaeken J, Matthijs G. 2008. Deficiencies in subunits of the
632 Conserved Oligomeric Golgi (COG) complex define a novel group of Congenital
633 Disorders of Glycosylation. Molecular Genetics and Metabolism 93:15–21.
634 28. Shestakova A, Zolov S, Lupashin V. 2006. COG Complex-Mediated Recycling of Golgi
635 Glycosyltransferases is Essential for Normal Protein Glycosylation: COG Complex and
636 Golgi Glycosylation. Traffic 7:191–204.
637 29. Zolov SN, Lupashin VV. 2005. Cog3p depletion blocks vesicle-mediated Golgi retrograde
638 trafficking in HeLa cells. J Cell Biol 168:747–759.
639 30. Bailey Blackburn J, Pokrovskaya I, Fisher P, Ungar D, Lupashin VV. 2016. COG
640 Complex Complexities: Detailed Characterization of a Complete Set of HEK293T Cells
641 Lacking Individual COG Subunits. Front Cell Dev Biol 4.
642 31. Strauss JH, Strauss EG. 1994. The alphaviruses: gene expression, replication, and
643 evolution. Microbiol Rev 58:491–562.
644 32. Li Y, Muffat J, Omer Javed A, Keys HR, Lungjangwa T, Bosch I, Khan M, Virgilio MC,
645 Gehrke L, Sabatini DM, Jaenisch R. 2019. Genome-wide CRISPR screen for Zika virus
646 resistance in human neural cells. Proc Natl Acad Sci USA 116:9527–9532.
647 33. Tanaka A, Tumkosit U, Nakamura S, Motooka D, Kishishita N, Priengprom T, Sa-
648 ngasang A, Kinoshita T, Takeda N, Maeda Y. 2017. Genome-Wide Screening Uncovers
649 the Significance of N-Sulfation of Heparan Sulfate as a Host Cell Factor for Chikungunya
650 Virus Infection. J Virol 91:e00432-17, /jvi/91/13/e00432-17.atom.
651 34. Savidis G, McDougall WM, Meraner P, Perreira JM, Portmann JM, Trincucci G, John SP,
652 Aker AM, Renzette N, Robbins DR, Guo Z, Green S, Kowalik TF, Brass AL. 2016.
653 Identification of Zika Virus and Dengue Virus Dependency Factors using Functional
654 Genomics. Cell Rep 16:232–246.

655 35. Klimstra WB, Ryman KD, Johnston RE. 1998. Adaptation of Sindbis Virus to BHK Cells
656 Selects for Use of Heparan Sulfate as an Attachment Receptor. Journal of Virology
657 72:7357–7366.
658 36. Mislick KA, Baldeschwieler JD. 1996. Evidence for the role of proteoglycans in cation-
659 mediated gene transfer. Proceedings of the National Academy of Sciences 93:12349–
660 12354.
661 37. Payne CK, Jones SA, Chen C, Zhuang X. 2007. Internalization and Trafficking of Cell
662 Surface Proteoglycans and Proteoglycan-Binding Ligands. Traffic 8:389–401.
663 38. Jae LT, Raaben M, Riemersma M, van Beusekom E, Blomen VA, Velds A, Kerkhoven
664 RM, Carette JE, Topaloglu H, Meinecke P, Wessels MW, Lefeber DJ, Whelan SP, van
665 Bokhoven H, Brummelkamp TR. 2013. Deciphering the Glycosylome of
666 Dystroglycanopathies Using Haploid Screens for Lassa Virus Entry. Science 340:479–
667 483.
668 39. Blackburn JB, Kudlyk T, Pokrovskaya I, Lupashin VV. 2018. More than just sugars:
669 Conserved oligomeric Golgi complex deficiency causes glycosylation-independent
670 cellular defects. Traffic 19:463–480.
671 40. Ungar D, Oka T, Brittle EE, Vasile E, Lupashin VV, Chatterton JE, Heuser JE, Krieger
672 M, Waters MG. 2002. Characterization of a mammalian Golgi-localized protein complex,
673 COG, that is required for normal Golgi morphology and function. The Journal of Cell
674 Biology 157:405–415.
675 41. D'Souza Z, Blackburn JB, Kudlyk T, Pokrovskaya ID, Lupashin VV. 2019. Defects in
676 COG-Mediated Golgi Trafficking Alter Endo-Lysosomal System in Human Cells. Front
677 Cell Dev Biol 7:118.
678 42. Climer LK, Pokrovskaya ID, Blackburn JB, Lupashin VV. 2018. Membrane detachment
679 is not essential for COG complex function. MBoC 29:964–974.
680 43. Blackburn JB, Lupashin VV. 2016. Creating Knockouts of Conserved Oligomeric Golgi
681 Complex Subunits Using CRISPR-Mediated Gene Editing Paired with a Selection
682 Strategy Based on Glycosylation Defects Associated with Impaired COG Complex
683 Function, p. 145–161. *In* Brown, WJ (ed.), The Golgi Complex. Springer New York, New
684 York, NY.
685 44. López P, Girardi E, Mounce BC, Weiss A, Chane-Woon-Ming B, Messmer M, Kaukinen
686 P, Kopp A, Bortolamiol-Becet D, Fendri A, Vignuzzi M, Brino L, Pfeffer S. 2020. High-
687 throughput fluorescence-based screen identifies the neuronal microRNA miR-124 as a
688 positive regulator of alphavirus infection. J Virol JVI.02145-19, jvi;JVI.02145-19v1.

689 45. Boussif O, Lezoualc'h F, Zanta MA, Mergny MD, Scherman D, Demeneix B, Behr JP.
690 1995. A versatile vector for gene and oligonucleotide transfer into cells in culture and in
691 vivo: polyethylenimine. Proc Natl Acad Sci USA 92:7297–7301.
692 46. Schindelin J, Arganda-Carreras I, Frise E, Kaynig V, Longair M, Pietzsch T, Preibisch S,
693 Rueden C, Saalfeld S, Schmid B, Tinevez J-Y, White DJ, Hartenstein V, Eliceiri K,
694 Tomancak P, Cardona A. 2012. Fiji: an open-source platform for biological-image
695 analysis. Nat Methods 9:676–682.
696 47. Sievers F, Wilm A, Dineen D, Gibson TJ, Karplus K, Li W, Lopez R, McWilliam H,
697 Remmert M, Söding J, Thompson JD, Higgins DG. 2011. Fast, scalable generation of
698 high-quality protein multiple sequence alignments using Clustal Omega. Mol Syst Biol
699 7:539.
700

701 **Figures legends**

702 **Figure 1. CRISPR-Cas9 survival screen to long dsRNA identifies the extracellular**
703 **heparan-sulfates as necessary for nucleic acids internalization and cell death induction.**
704 **A.** Schematic representation of the CRISPR-Cas9 approach. HCT116 cells stably expressing a
705 human codon-optimized *S. pyogenes* Cas9 protein were transduced with the lentiviral sgRNA
706 library Brunello (MOI 0.3). 60.10^6 cells transduced cells were selected with 1 μg/mL
707 puromycin to obtain a mutant cell population to cover at least 300× the library. Selective
708 pressure via synthetic long dsRNA (1 μg/mL) was applied to induce cell death (in red). DNA
709 libraries from input cells and cells surviving the dsRNA treatment as three independent
710 biological replicates were sequenced on an Illumina HiSeq4000. Comparison of the relative
711 sgRNA boundance in the Input and dsRNA condition were done using the MAGeCK standard
712 pipeline. **B.** Median normalized read count distribution of all sgRNAs for the Input (in black)
713 and dsRNA (in red) replicates**. C.** Bubble plot of the candidate genes. Significance of RRA
714 score was calculated for each gene in the dsRNA condition compared to INPUT using the
715 MAGeCK software. The number of enriched sgRNAs for each gene is represented by the
716 bubble size. The gene ontology pathways associated to the significant top hits are indicated in
717 orange and green. **D.** Viability assay. Cells were transfected (80 000 cells; 1 μg/mL) or
718 nucleofected (200 000 cells; 400 ng) with synthetic long dsRNA and cell viability was
719 quantified 24 h (nucleofection) or 48 h (transfection) post treatment using PrestoBlue reagent.
720 Average of at least three independent biological experiments +/- SD is shown. One-way
721 ANOVA analysis, * $p < 0.05$. **E-F.** Cy5-labeled dsRNA (80 000 cells; 1 μg/mL) was transfected
722 into HCT116cas9, B4GALT7#1 and 2, SLC35B2#1 and #2 cells and Cy5 fluorescence was
723 quantified using FACS (10 000 events). The relative number of the Cy5 positive (Cy5+) cells
724 (**E**) and the relative median of Cy5 intensity of fluorescence (**F**) compared to HCT116cas9 cells
725 are shown. Average of three independent biological experiments +/- SD are shown. Paired t.test

726 analysis, * $p < 0.05$. **G.** Quantification of extracellular heparan-sulfates. FACS analysis of
727 HCT116 control or KO clones stained with the HS-specific antibody 10E4 (in red) compared
728 to unstained samples (in blue) (10 000 events). One representative experiment out of three is
729 shown.
730
731 **Figure 2. *COG4* is a novel host susceptibility factor to long dsRNA induced cell death.**
732 **A.** Viability assay. Cells (80 000 cells; 1 μg/mL) were transfected with dsRNA then the
733 viability of the cells was quantified 48 h post transfection using PrestoBlue reagent. Data from
734 at least three independent biological experiments are shown. One-way ANOVA analysis, * $p <$
735 0.05. **B-C.**Cy5-labeled dsRNA transfection (80 000 cells; 1 μg/mL) in HEK293T, KO COG4
736 and rescued cells. Cy5 fluorescence was quantified using FACSCalibur (10 000 events). The
737 percentage of Cy5+ cells (**B**) and the relative median of Cy5 intensity of fluorescence (**C**)
738 compared to parental HEK293T cells is shown. Average of three experiments +/- SD are shown.
739 Paired t.test analysi analysis, * $p < 0.05$. **D-E.** qPCR quantification of dsRNA and IFN-β. Cells
740 (300 000 cells; 1 μg/mL) were transfected with synthetic long dsRNA. Total RNA was
741 extracted 24 h post transfection and quantified by RT-qPCR. The histogram represents the
742 expression fold change of synthetic dsRNA (**D**) and IFN- β mRNA (**E**) relative to GAPDH
743 mRNA in dsRNA transfected HEK293T KO COG4 rescued compared to HEK293T KO
744 COG4. Average of three independent biological experiments +/- SD are shown. Paired t.test
745 analysis, * $p < 0.05$. **F-G.** poly I:C rhodamine transfection and immunofluorescence in
746 HEK293T and HEK293T KO COG4. Cells were transfected with rhodamine-labeled poly I:C
747 (in red) and with a Rab5-GFP plasmid (in green). Images were acquired using a spinning disk
748 microscope at different time post transfection. Representative pictures (**E)** and the
749 approximative number of rhodamine-positive foci per cells quantified by counting 7 fields per
750 conditions (**F**) are shown. Two-way ANOVA analysis, * $p < 0.05$.

751

752 **Figure 3. CRISPR-Cas9 screen identifies *COG4* as a permissivity factor to SINV**

753 **A.** Schematic representation of the CRISPR-Cas9 approach. HCT116 cells stably expressing a
754 human codon-optimized *S. pyogenes* Cas9 protein were transduced with the lentiviral sgRNA
755 library Brunello (MOI 0.3). 60.10^6 transduced cells were selected with 1 µg/mL puromycin to
756 obtain a mutant cell population to cover at least 300X the library. Selective pressure via SINV
757 infection (MOI 0.1) was applied to induce cell death (in red). DNA libraries from input cells
758 and cells surviving the dsRNA treatment as three independent biological replicates were
759 sequenced on an Illumina HiSeq4000. Comparison of the relative sgRNA boundance in the
760 Input and dsRNA condition were done using the MAGeCK standard pipeline

761 **B.** Median normalized read count distribution of all sgRNAs for the Input (in black) and SINV
762 (in red) replicates**. C.** Bubble plot of the candidate genes. Significance of RRA score was
763 calculated for each gene in the dsRNA condition compared to INPUT using the MAGeCK
764 software. The number of enriched sgRNAs for each gene is represented by the bubble size. The
765 gene ontology pathways associated to the significant top hits are indicated in orange and green.

766 **D.** Viability of cells upon SINV infection. Cells were infected with SINV at MOI of 0.1 then
767 the viability of the cells was quantified 24, 48 and 72 h post infection using PrestoBlue reagent.
768 One-way ANOVA analysis, * $p < 0.05$. **D.** SINV-GFP plaque assay. WT, COG4KO and
769 rescued HEK293T cells were infected with SINV-GFP for 24 and 48h at MOI of 1 and
770 supernatant was collected in order to measure viral production. The fold change in titer relative
771 to HEK293T arbitrarily set to 1 is shown. Average of three independent biological experiments
772 +/- SD is shown. Paired t.test analysis * $p < 0.05$.

773

774

775 **Supplemental information**

776

777 **Supplemental figures legends**

778 **Figure S1. Set up of the HCT116 cells as model for SINV infection and dsRNA-induced**
779 **cell death.**

780 **A.** Representative pictures of HCT116cas9 cells uninfected or infected with SINV-GFP MOI
781 of 1 at 24 and 48h post infection (hpi). 5× optical microscopy**. B.** Representative pictures of
782 HCT116cas9 cells at 24 and 48h post dsRNA (80 000 cells; 1 μg/mL) compared to non
783 transfected ones. 5X optical microscopy. **C.** Western blot of FLAG-Cas9 expression in
784 HCT116cas9 cells. Antibody against FLAG and GAPDH (normalizer) were used. **D-E**.
785 Distribution of sgRNA normalized read counts of selected genes. The read counts for the four
786 individual sgRNAs targeting enriched (*SLC35B2, BGAL4T7, COG4*) and not enriched genes
787 (*DDX58*, negative control) in the dsRNA samples (**D**) and in the SINV samples (**E**) over the
788 Input are shown.

789

790 **Figure S2. Generation of SLC35B2 and B4GALT7 HCT116 CRISPR/Cas9 knock-out**
791 **monoclonal cell lines.**

792 **A.** PCR screen of *SLC35B2* and *B4GALT7* knock-out clones obtained by CRISPR/Cas9. The
793 gels show the amplicons corresponding to wild type and deleted alleles that were subsequently
794 sequenced. **B.** Clustal Omega (47) alignment of the wild type and mutated peptide sequences
795 corresponding to the genomic deletions identified in the different clones. The reference
796 aminoacidic sequence is represented in yellow (unknown domains - InterPro) and orange
797 (known domains – InterPro). The peptidic sequences resulting in shorter protein due to
798 deletions or formation of premature stop codon in the knock-out clones are represented with
799 black bars or red rectangles, respectively.

800

801 **Figure S3**: **GFP plasmid transfectability in SLC35B2 and B4GALT7 HCT116**
802 **CRISPR/Cas9 KO cells.**

803 **A.** Representative pictures of GFP plasmid transfectability assay. Cells were transfected
804 (80 000 cells; 2 μg/mL) or nucleofected (200 000 cells; 500 ng) with a plasmid coding for GFP
805 and the GFP positive cells were observed by fluorescence microscopy at 24h (nucleofection)
806 or 48h (transfection) post treatment. Pictures were taken at 10× magnification, scale bar
807 represents 50 μm. **B.** GFP transfectability by FACS analysis. The different cell types were
808 transfected (80 000 cells; 2 μg/mL) with plasmid coding for GFP for 48h. The percentage of
809 GFP+ cells were determined by FACS analysis using a FACSCalibur. **C-D-E.** DNA plasmid
810 transfectability assay upon heparan-sulfates depletion. Cells were treated with 50 mM sodium
811 chlorate or with 2 units of heparinase then transfected with GFP plasmid. The relative number
812 of GFP positive (GFP+) cells (**C**), the GFP intensity of fluorescence (**D**) and the relative median
813 intensity of fluorescence of extracellular heparan-sulfates (HS) staining (**E**) were quantified
814 48h post transfection using FACS (10 000 events). Data from at least three independent
815 biological experiments +/- SD are shown. Paired t.test analysis, * $p < 0.05$.

816

817 **Figure S4. Characterization of the survival phenotype in HCT116 KO COG4 and**
818 **HEK293 KO COG4 cells.**

819 **A.** Viability assay. HCT116cas9 and HCT116cas9 KO COG4 cells (80 000 cells; 1 μg/mL)
820 were transfected with dsRNA then the cell viability was quantified 48 h post transfection using
821 PrestoBlue reagent. Data from at least three independent biological experiments are shown.
822 Paired t.test analysis, * $p < 0.05$. **B-C.** Cy5-labeled dsRNA transfection (80 000 cells; 1 μg/mL)
823 in HCT116cas9 and HCT116cas9 KO COG4 cells. Cy5 fluorescence was quantified using
824 FACSCalibur (10 000 events). The relative number of Cy5+ cells (**B**) and the relative median

825 of Cy5 intensity of fluorescence (**C**) compared to parental HCT116cas9 cells is shown. Average
826 of three experiments +/- SD are shown. Paired t.test analysis, * $p < 0.05$. **D.** Quantification of
827 extracellular heparan-sulfates. Upper panel correspond to FACS analysis of HEK293T control
828 (WT & rescued – respectively in red and orange) or HEK293T KO *COG4* (in blue) cells stained
829 with the HS-specific antibody 10E4 and lower panel show the unstained sample and HEK293T
830 KO *COG4*. One representative experiment out of three is shown. (10 000 events) **E-F.** GFP
831 transfectability by FACS analysis. HEK293T and HEK293T KO *COG4* cells were transfected
832 (80 000 cells; 2 μg/mL) with plasmid coding for GFP for 48h. The percentage of GFP+ cells
833 (**E**) and the relative median of GFP intensity of fluorescence (**F**) compared to parental
834 HEK293T cells was determined by FACS analysis using a FACSCalibur. Average of three
835 experiments +/- SD are shown Paired t.test analysis, * $p < 0.05$.
836
837 **Figure S5. Accumulation of GFP and dsRNA upon SINV infection in presence or absence**
838 **of COG4. A.** Representative pictures of HEK293T and HEK293T KO COG4 cells infected
839 with SINV-GFP MOI of 0.1 at 24 and 48h post infection (hpi). Pictures were taken at 20x
840 magnification. One representative experiment out of three is shown. **B.** DsRNA
841 immunofluorescence assay. Cells were infected with SINV at MOI of 0.1 for 24 h, then fixed
842 and stained with J2 antibody, which recognizes dsRNA longer than 40bp and DAPI to stain the
843 nuclei. Pictures were taken at 40× magnification with BX51 (Olympus) microscope.
844
845 **Table S1**
846 List of primers used in the study.
847 **Dataset S1**
848 Count of sequenced sgRNA per genes in every replicates
849 **Dataset S2**

850 MAGeCK comparison report enriched sgRNAs in dsRNA versus Input samples

851 **Dataset S3**

852 MAGeCK comparison report enriched sgRNAs in SINV versus Input samples

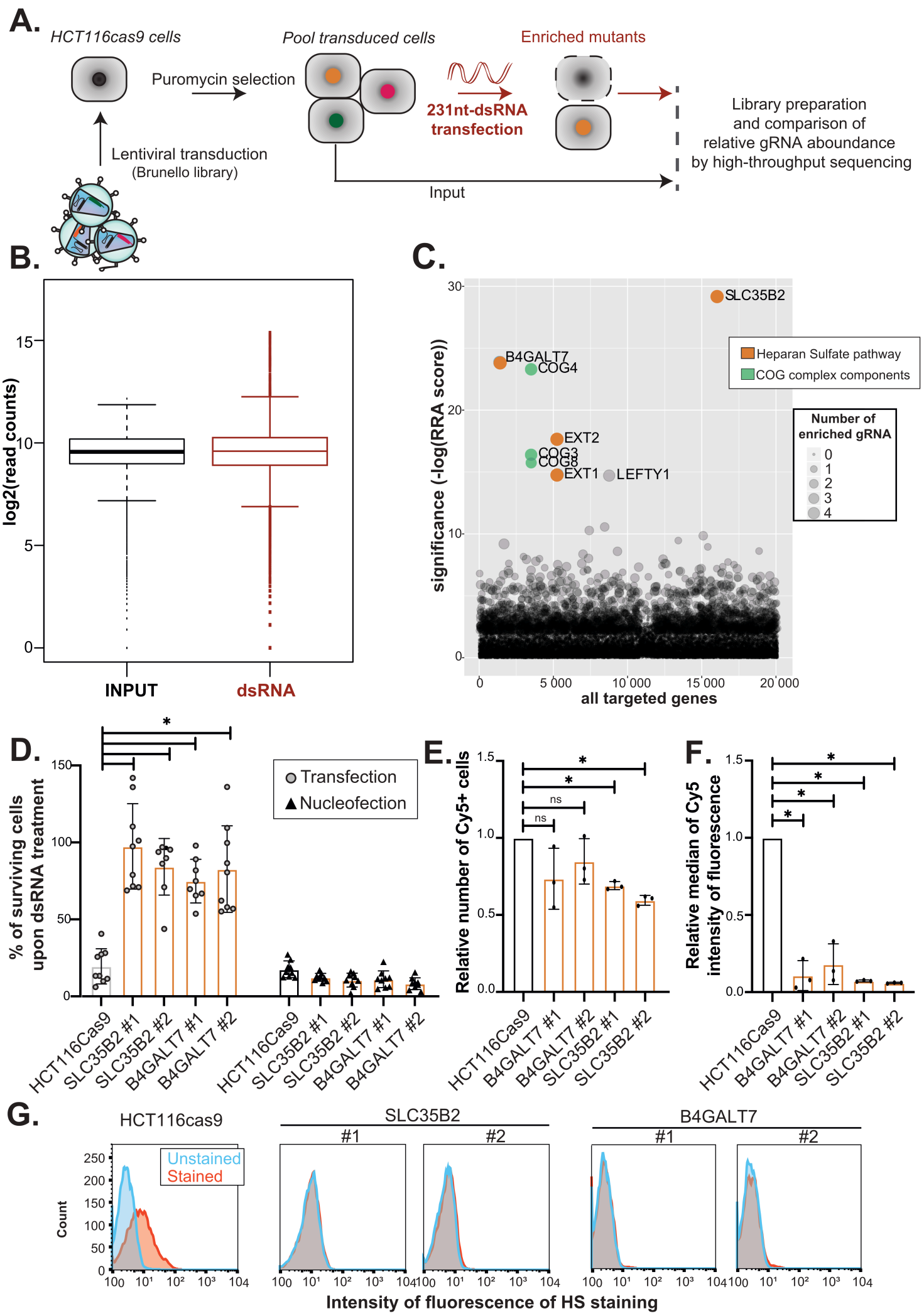
A.
HCT116cas9 cells
Puromycin selection
Pool transduced cells
231nt-dsRNA transfection
Enriched mutants
Library preparation and comparison of relative gRNA aboundance by high-throughput sequencing
Lentiviral transduction (Brunello library)
Input
B.
log2(read counts)
INPUT
dsRNA
C.
significance (-log(RRA score))
all targeted genes
SLC35B2
B4GALT7
COG4
EXT2
COG3
COG8
EXT1
LEFTY1
Heparan Sulfate pathway
COG complex components
Number of enriched gRNA
D.
% of surviving cells upon dsRNA treatment
Transfection
Nucleofection
HCT116Cas9
SLC35B2 #1
SLC35B2 #2
B4GALT7 #1
B4GALT7 #2
E.
Relative number of Cy5+ cells
ns
F.
Relative median of Cy5 intensity of fluorescence
G.
HCT116cas9
SLC35B2
B4GALT7
Unstained
Stained
Count
Intensity of fluorescence of HS staining

Figure 1

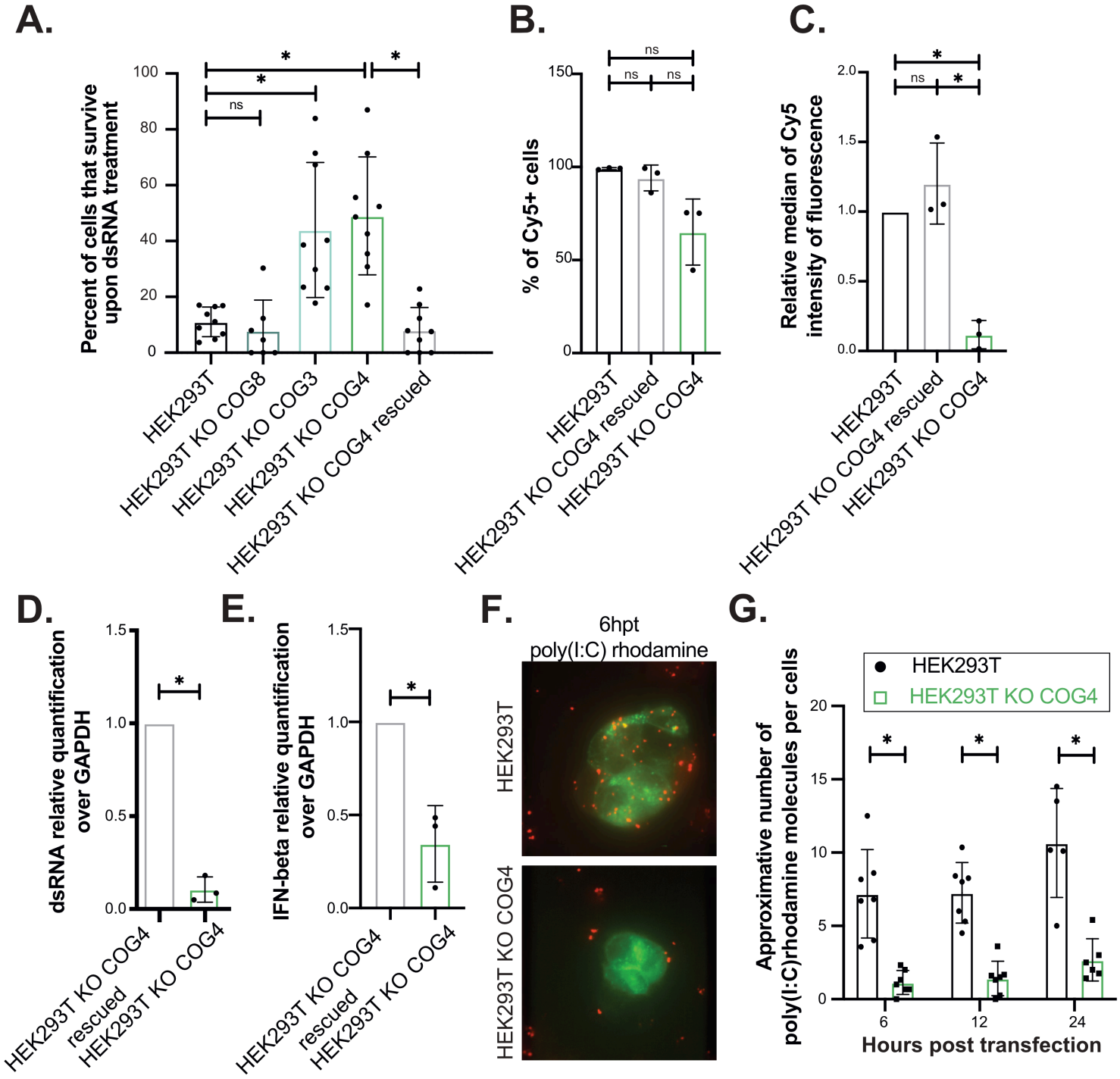
A.
Percent of cells that survive upon dsRNA treatment
100
80
60
40
20
0
*
*
*
ns
HEK293T
HEK293T KO COG8
HEK293T KO COG3
HEK293T KO COG4
HEK293T KO COG4 rescued
B.
% of Cy5+ cells
150
100
50
0
ns
ns
ns
HEK293T
HEK293T KO COG4 rescued
HEK293T KO COG4
C.
Relative median of Cy5 intensity of fluorescence
2.0
1.5
1.0
0.5
0.0
*
ns
*
HEK293T
HEK293T KO COG4 rescued
HEK293T KO COG4
D.
dsRNA relative quantification over GAPDH
1.5
1.0
0.5
0.0
*
HEK293T KO COG4 rescued
HEK293T KO COG4
E.
IFN-beta relative quantification over GAPDH
1.5
1.0
0.5
0.0
*
HEK293T KO COG4 rescued
HEK293T KO COG4
F.
6hpt
poly(I:C) rhodamine
HEK293T
HEK293T KO COG4
G.
HEK293T
HEK293T KO COG4
Approximative number of poly(I:C)rhodamine molecules per cells
20
15
10
5
0
*
*
*
6
12
24
Hours post transfection

Figure 2

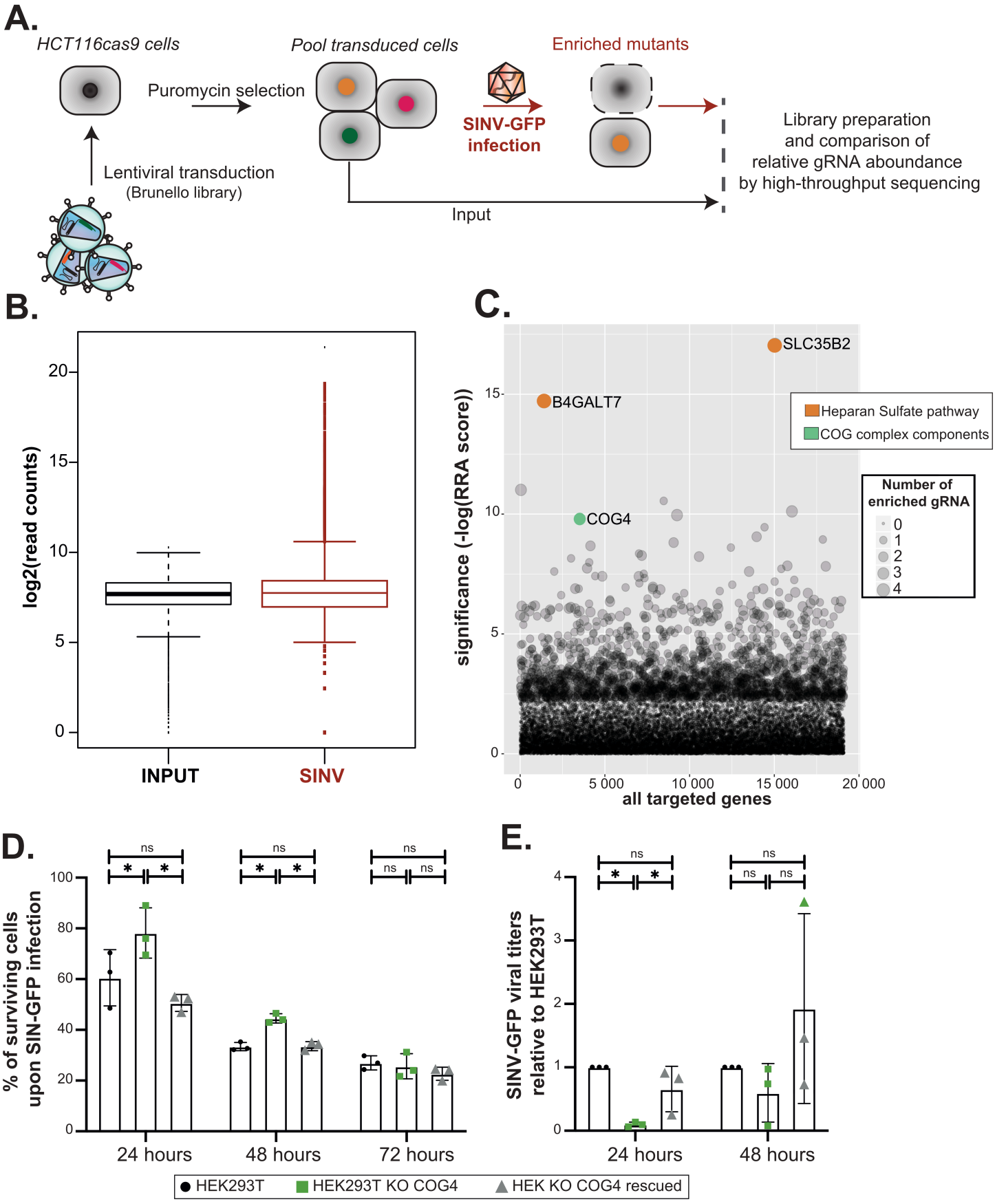
A.
HCT116cas9 cells
Puromycin selection
Pool transduced cells
Enriched mutants
SINV-GFP infection
Lentiviral transduction (Brunello library)
Input
Library preparation and comparison of relative gRNA aboundance by high-throughput sequencing
B.
log2(read counts)
INPUT
SINV
C.
significance (-log(RRA score))
all targeted genes
SLC35B2
B4GALT7
COG4
Heparan Sulfate pathway
COG complex components
Number of enriched gRNA
D.
% of surviving cells upon SIN-GFP infection
24 hours
48 hours
72 hours
ns
E.
SINV-GFP viral titers relative to HEK293T
HEK293T
HEK293T KO COG4
HEK KO COG4 rescued

Figure 3

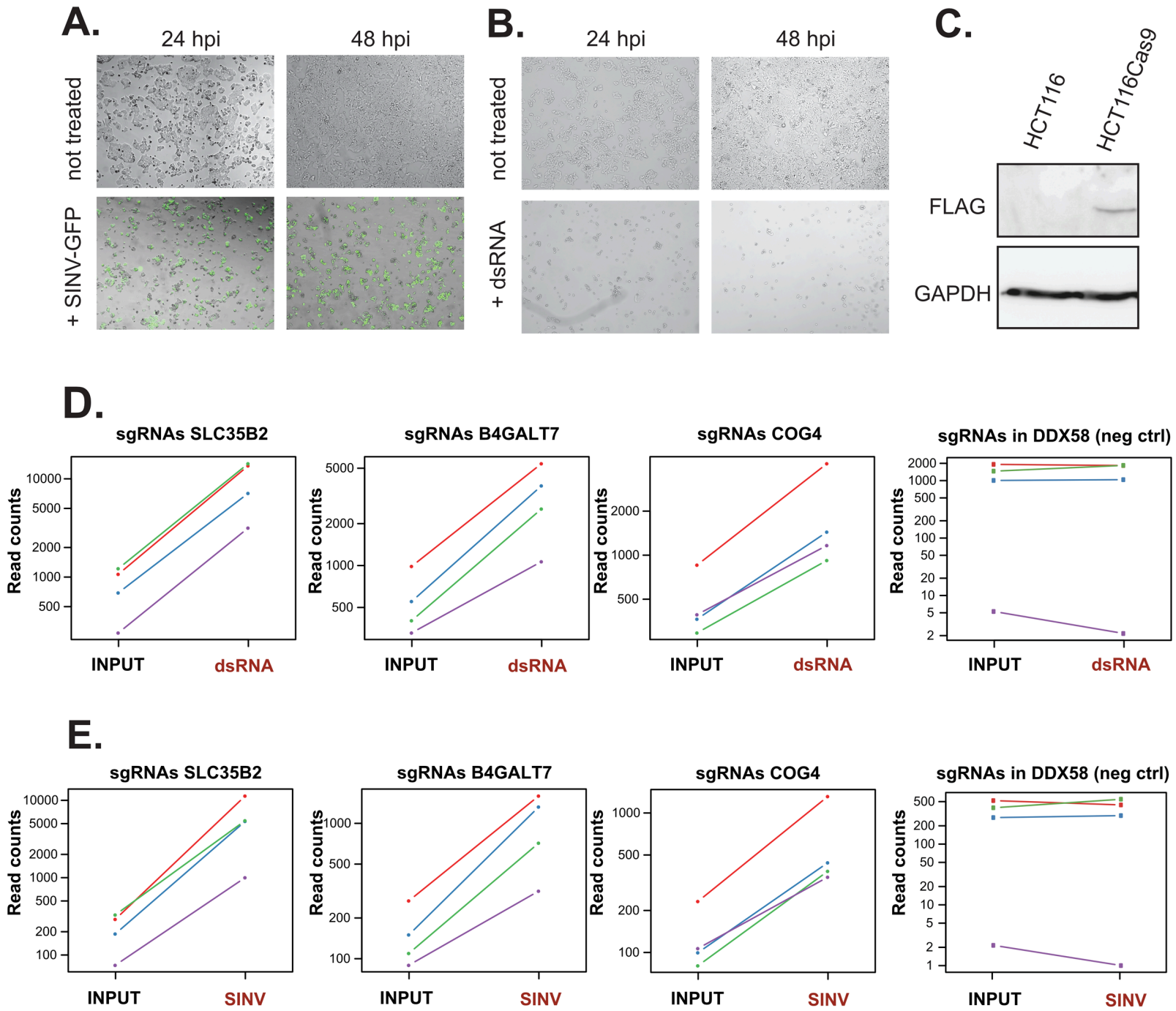
A.
24 hpi
48 hpi
not treated
+ SINV-GFP
B.
24 hpi
48 hpi
not treated
+ dsRNA
C.
HCT116
HCT116Cas9
FLAG
GAPDH
D.
sgRNAs SLC35B2
sgRNAs B4GALT7
sgRNAs COG4
sgRNAs in DDX58 (neg ctrl)
Read counts
INPUT
dsRNA
E.
sgRNAs SLC35B2
sgRNAs B4GALT7
sgRNAs COG4
sgRNAs in DDX58 (neg ctrl)
Read counts
INPUT
SINV

Figure S1

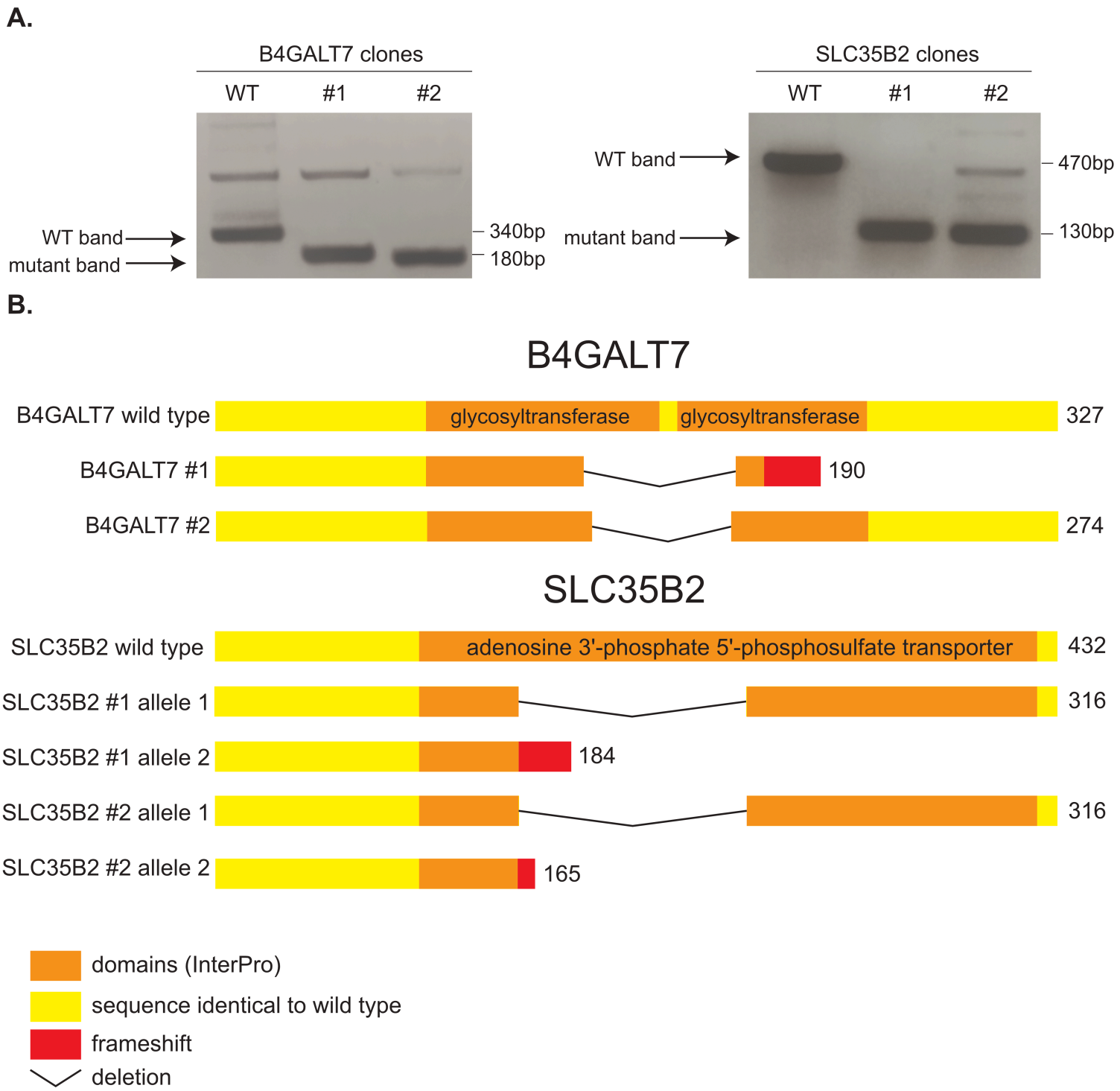
A.
B4GALT7 clones
WT
#1
#2
WT band
mutant band
340bp
180bp
SLC35B2 clones
WT
#1
#2
WT band
mutant band
470bp
130bp
B.
B4GALT7
B4GALT7 wild type
glycosyltransferase
glycosyltransferase
327
B4GALT7 #1
190
B4GALT7 #2
274
SLC35B2
SLC35B2 wild type
adenosine 3'-phosphate 5'-phosphosulfate transporter
432
SLC35B2 #1 allele 1
316
SLC35B2 #1 allele 2
184
SLC35B2 #2 allele 1
316
SLC35B2 #2 allele 2
165
domains (InterPro)
sequence identical to wild type
frameshift
deletion

Figure S2

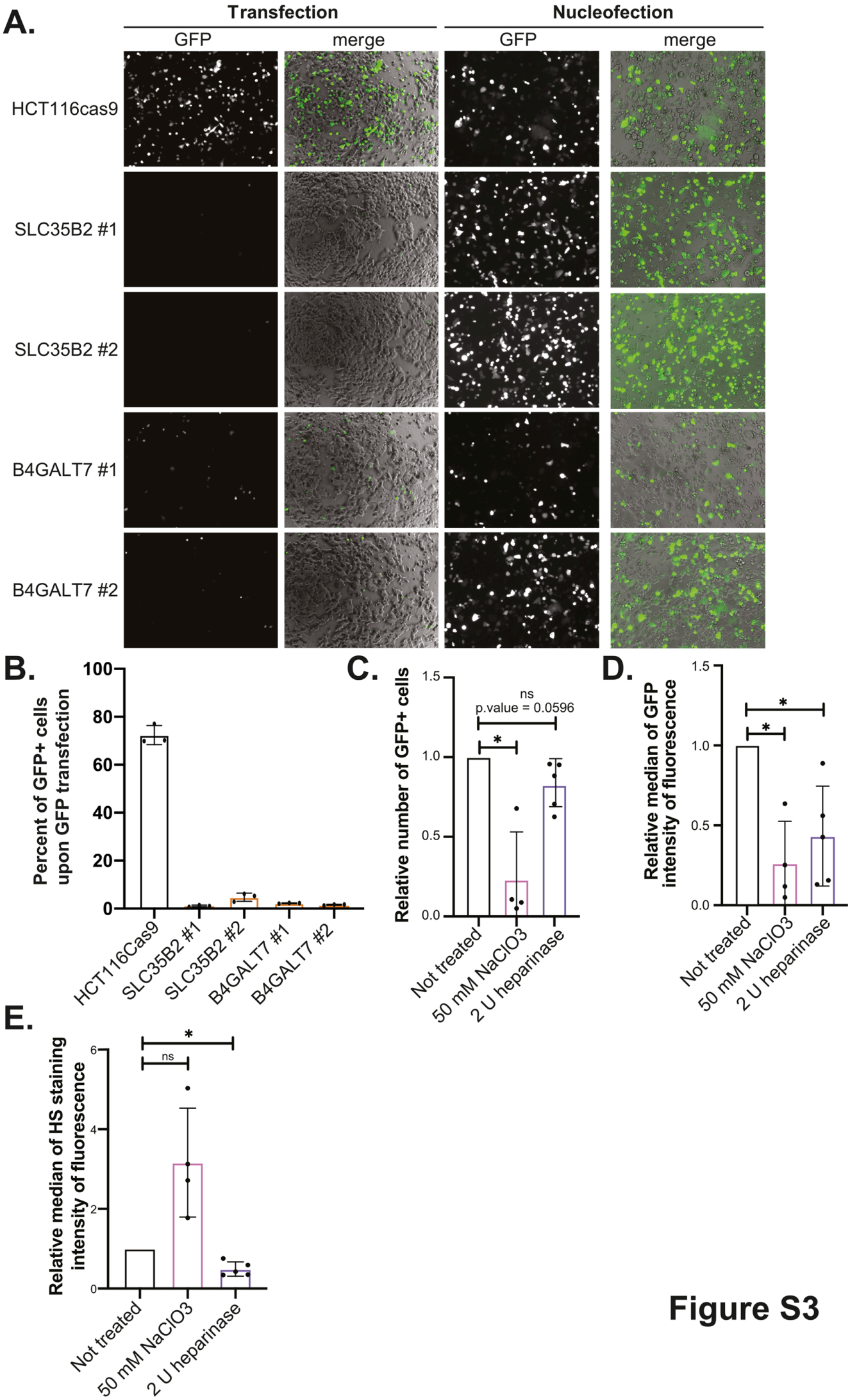
A.
Transfection
Nucleofection
GFP
merge
GFP
merge
HCT116cas9
SLC35B2 #1
SLC35B2 #2
B4GALT7 #1
B4GALT7 #2
B.
Percent of GFP+ cells upon GFP transfection
100
80
60
40
20
0
HCT116Cas9
SLC35B2 #1
SLC35B2 #2
B4GALT7 #1
B4GALT7 #2
C.
Relative number of GFP+ cells
1.5
1.0
0.5
0.0
ns
p.value = 0.0596
*
Not treated
50 mM NaClO3
2 U heparinase
D.
Relative median of GFP intensity of fluorescence
1.5
1.0
0.5
0.0
*
*
Not treated
50 mM NaClO3
2 U heparinase
E.
Relative median of HS staining intensity of fluorescence
6
4
2
0
*
ns
Not treated
50 mM NaClO3
2 U heparinase

Figure S3

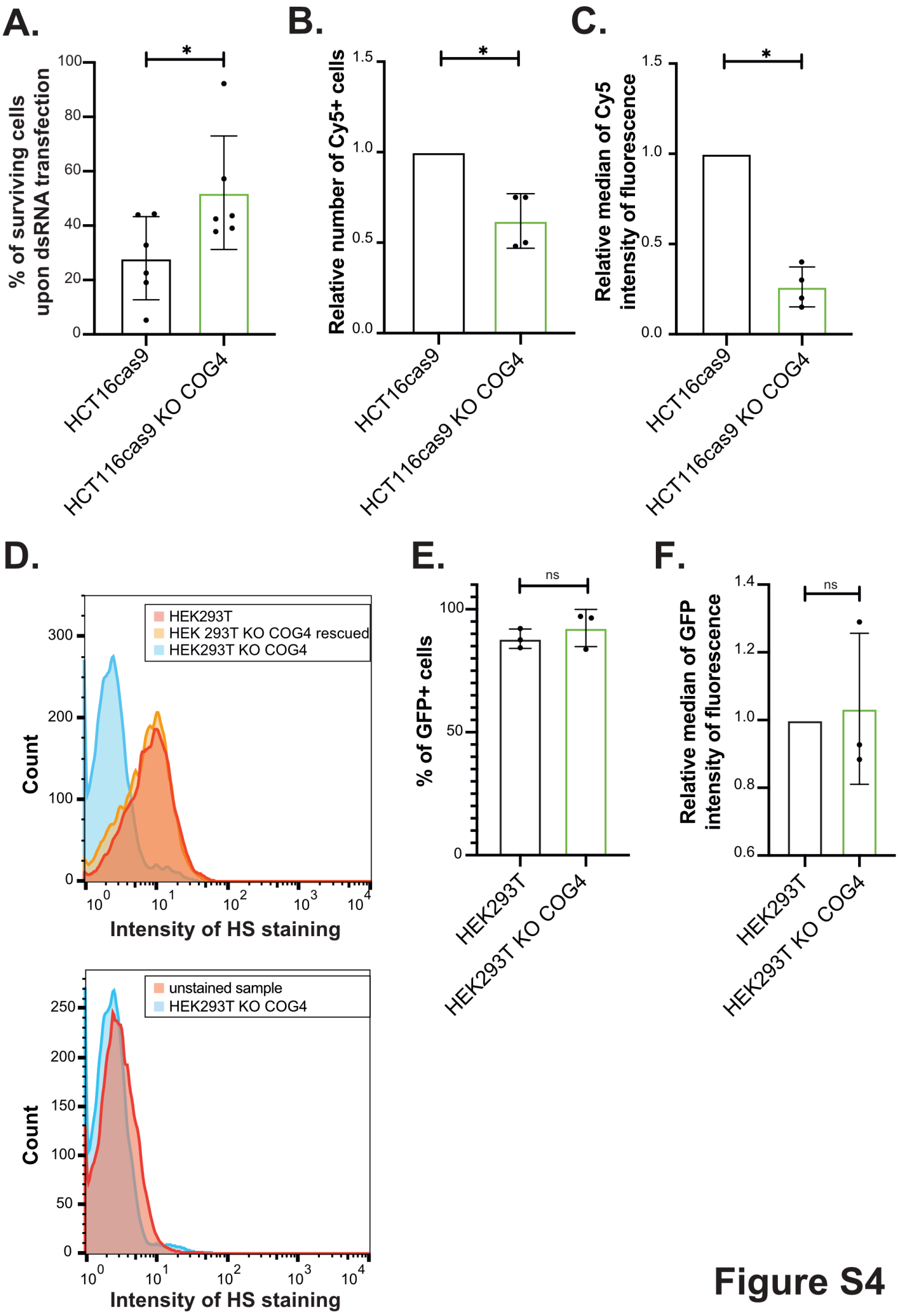
A.
% of surviving cells upon dsRNA transfection
100
80
60
40
20
0
*
HCT16cas9
HCT116cas9 KO COG4
B.
Relative number of Cy5+ cells
1.5
1.0
0.5
0.0
*
HCT16cas9
HCT116cas9 KO COG4
C.
Relative median of Cy5 intensity of fluorescence
1.5
1.0
0.5
0.0
*
HCT16cas9
HCT116cas9 KO COG4
D.
HEK293T
HEK 293T KO COG4 rescued
HEK293T KO COG4
Count
300
200
100
0
10^0
10^1
10^2
10^3
10^4
Intensity of HS staining
unstained sample
HEK293T KO COG4
Count
250
200
150
100
50
0
10^0
10^1
10^2
10^3
10^4
Intensity of HS staining
E.
% of GFP+ cells
100
50
0
ns
HEK293T
HEK293T KO COG4
F.
Relative median of GFP intensity of fluorescence
1.4
1.2
1.0
0.8
0.6
ns
HEK293T
HEK293T KO COG4

Figure S4

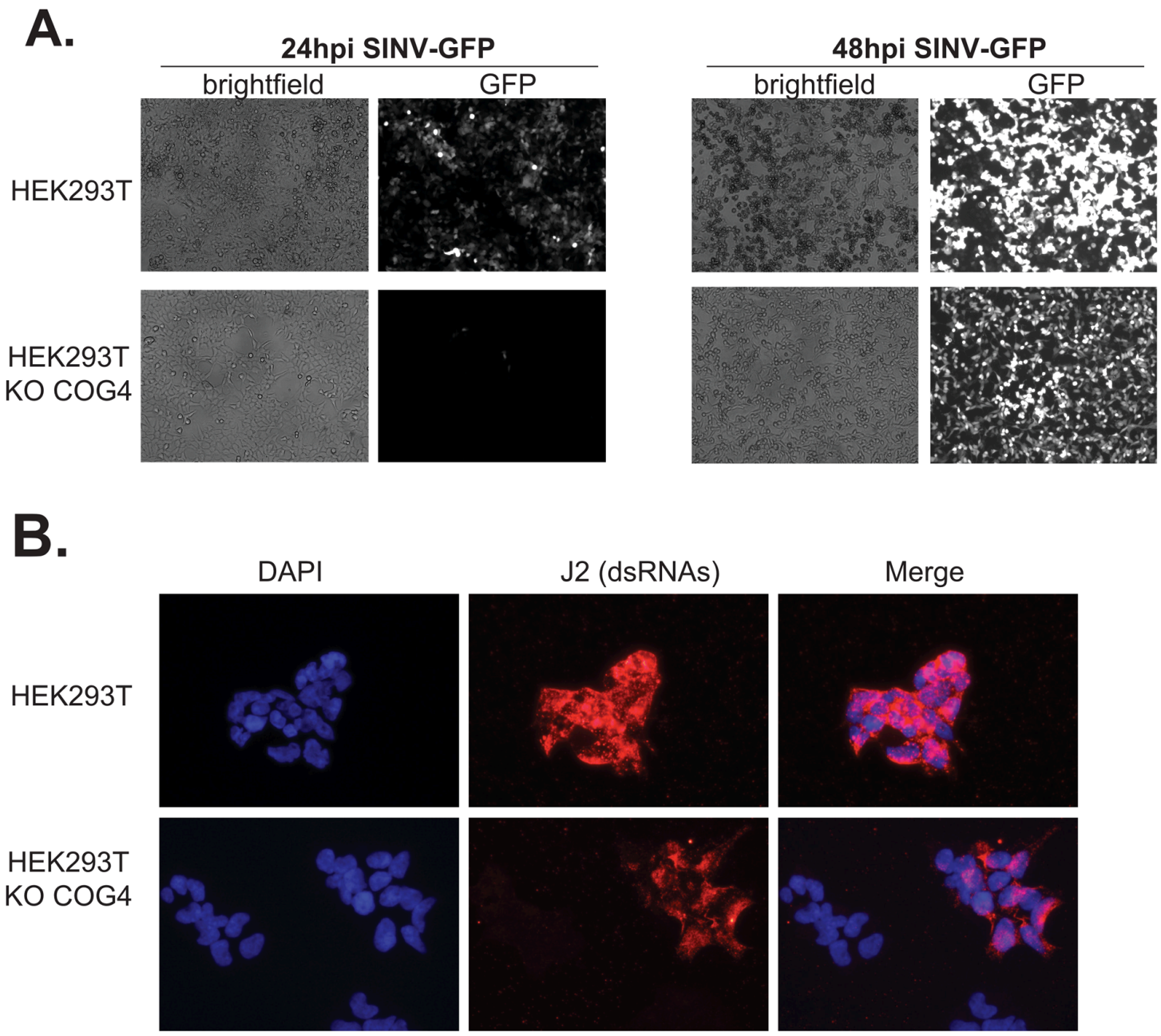
A.
24hpi SINV-GFP
48hpi SINV-GFP
brightfield
GFP
brightfield
GFP
HEK293T
HEK293T
KO COG4
B.
DAPI
J2 (dsRNAs)
Merge
HEK293T
HEK293T
KO COG4

Figure S5